

See discussions, stats, and author profiles for this publication at: <https://www.researchgate.net/publication/236055264>

Phenylpropiophenone derivatives as potential anticancer agents: Synthesis, biological evaluation and quantitative structure–activity relationship study

ARTICLE *in* EUROPEAN JOURNAL OF MEDICINAL CHEMISTRY · FEBRUARY 2013

Impact Factor: 3.45 · DOI: 10.1016/j.ejmech.2013.02.013 · Source: PubMed

CITATIONS

4

READS

73

7 AUTHORS, INCLUDING:



Katarina Nikolic

University of Belgrade

61 PUBLICATIONS 236 CITATIONS

SEE PROFILE



Radmila Novakovic

University of Belgrade

21 PUBLICATIONS 31 CITATIONS

SEE PROFILE

Accepted Manuscript

Phenylpropiophenone derivatives as potential anticancer agents: Synthesis, biological evaluation and quantitative structure-activity relationship study

Branka M. Ivković Katarina Nikolic, Bojana B. Ilić Š. oićak, Radmila B. Novaković Olivera A. Yudin, Sote M. Vladimirov



PII: S0223-5234(13)00099-8

DOI: [10.1016/j.ejmech.2013.02.013](https://doi.org/10.1016/j.ejmech.2013.02.013)

Reference: EJMECH 6003

To appear in: *European Journal of Medicinal Chemistry*

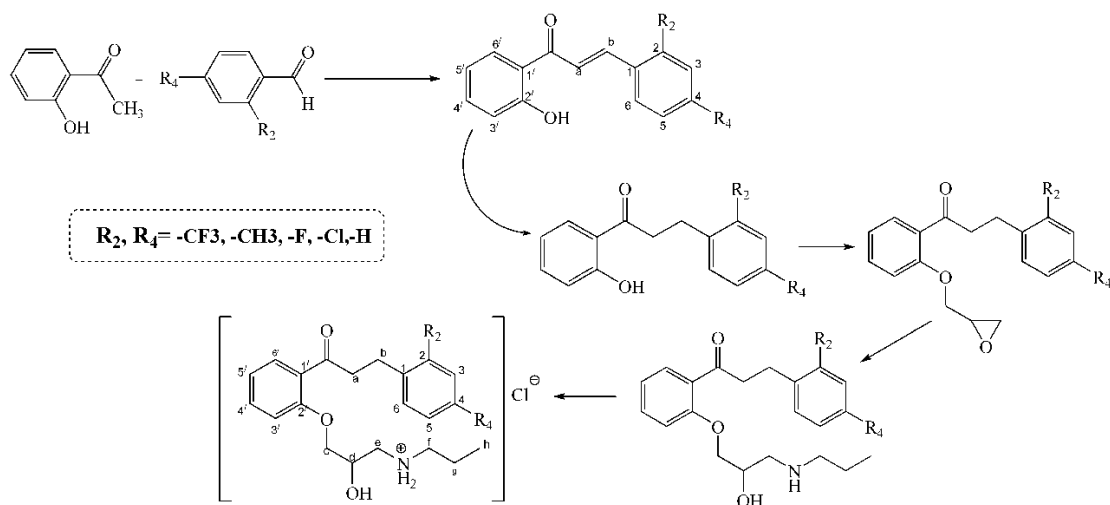
Received Date: 21 November 2012

Revised Date: 8 February 2013

Accepted Date: 12 February 2013

Please cite this article as: B.M. Ivković K. Nikolic, B.B. Ilić Š. oićak, R.B. Novaković O.A. Yudin, S.M. Vladimirov, Phenylpropiophenone derivatives as potential anticancer agents: Synthesis, biological evaluation and quantitative structure-activity relationship study, *European Journal of Medicinal Chemistry* (2013), doi: 10.1016/j.ejmech.2013.02.013.

This is a PDF file of an unedited manuscript that has been accepted for publication. As a service to our customers we are providing this early version of the manuscript. The manuscript will undergo copyediting, typesetting, and review of the resulting proof before it is published in its final form. Please note that during the production process errors may be discovered which could affect the content, and all legal disclaimers that apply to the journal pertain.



**Phenylpropiophenone derivatives as potential anticancer agents:
Synthesis, biological evaluation and quantitative structure-activity
relationship study**

Branka M. Ivković ^{1*}, Katarina Nikolic ¹, Bojana B. Ilić ², Željko S. Žižak ³, Radmila B. Novaković ⁴, Olivera A. Čudina¹, and Sote M. Vladimirov ¹

¹Department of Pharmaceutical Chemistry, Faculty of Pharmacy, University of Belgrade, Vojvode Stepe 450, 11000 Belgrade Serbia;

²Institute of Endocrinology, Diabetes and Metabolic Diseases, Medical School, University of Belgrade, Dr Subotica 13, 11000 Belgrade, Serbia;

³Institute of Oncology and Radiology of Serbia, Pasterova 14, 11000 Belgrade, Serbia;

⁴Department of Pharmacology, Clinical Pharmacology and Toxicology, Faculty of Medicine, University of Belgrade, Dr Subotica 8, 11000 Belgrade, Serbia

**Corresponding author:*

Branka Ivkovic,

Department of Pharmaceutical Chemistry, Faculty of Pharmacy, University of Belgrade , Vojvode Stepe 450, 11221 Belgrade-Kumodraz, P.O.Box 146, Serbia.

e-mail: blucic@pharmacy.bg.ac.rs

Phone : + 381 11 3951-335, Fax : + 381 11 3972-840

Abstract

Series of twelve chalcone and propafenone derivatives has been synthesized and evaluated for anticancer activities against HeLa, Fem-X, PC-3, MCF-7, LS174 and K562 cell lines. The 2D-QSAR and 3D-QSAR studies were performed for all compounds with cytotoxic activities against each cancer cell line. Partial least squares (PLS) regression has been applied for selection of the most relevant molecular descriptors and QSAR models building. Predictive potentials of the created 2D-QSAR and 3D-QSAR models for each cell line were compared, by use of leave-one-out cross-validation and external validation, and optimal QSAR models for each cancer cell line were selected. The QSAR studies have selected the most significant molecular descriptors and pharmacophores of the chalcone and propafenone derivatives and proposed structures of novel chalcone and propafenone derivatives with enhanced anticancer activity on the HeLa, Fem-X, PC-3, MCF-7, LS174 and K562 cells.

Keywords: Propafenone derivatives, Chalcones, QSAR, anticancer agents

1. Introduction

Cancer is the second leading cause of human death ^[1]. Although there are many therapeutic strategies, including chemotherapy and radiotherapy, high systemic toxicity and drug resistance are the main problems in the treatment of cancer. Therefore, scientists are focused on finding new therapeutic targets for cancer and discovering novel potent and selective antineoplastic drugs ^[2].

Since naturally occurring chalcones and their synthetic analogues, such as propafenone derivatives, displayed significant cytotoxic activity against various tumor cells ^[3-6] the main aim of this research was to develop new propafenone derivatives and chalcones with enhanced anticancer activity.

Apart from antineoplastic activity, chalcones displayed considerable chemoprotective, antiangiogenic, antibacterial, antifungal, antiparasitic, antioxidative, and anti-inflammatory activity ^[4].

Chemically, chalcones are 1, 3-diaryl-2-propen-1-ones with an enone system between two aromatic rings (Figure 1). They are precursors for the synthesis of various compounds (flavonoids, propafenone etc.) which exhibit interesting pharmacological activities ^[7-10].

Previously performed chalcones studies have shown that its ketovinyl moiety (-C(O)-C=C-) acts as *Michel* acceptor that preferential covalently binds reactive sulfhydryl (-SH) groups of biomolecules ^[11] in contrast to amino and hydroxy groups of the biomolecules ^[12-13] (Figure1). Therefore chalcones may cause lower incidence of typical side effects associated with a number of alkylating agents used in chemotherapy ^[14]. One of the proposed anticancer

mechanisms of chalcones is based on their structure similarity with colchicine. Actually, anticancer activity of chalcones is the result of their binding to tubulin and prevention of tubulin polymerization into microtubules ^[15].

On the other side, propafenone (Figure 1) belongs to Ic class of antiarrhythmic drugs that block the voltage-dependent cardiac sodium channels. Furthermore, propafenone inhibits: L-type of calcium channels, potassium channels, and β -adrenergic receptors in the heart ^[16]; the growth of cultured *Plasmodium falciparum* ^[17] and the membrane glycoprotein (P-glycoprotein (PGP)) involved in mediated drugs resistance (MDR) ^[5, 6, 18, 19].

Earlier pharmacological studies discovered that ion channels blockers selectively impair proliferation of cancer cells ^[20-22]. These observations were further confirmed by comprehensive studies on the functional implications of ion channels in the biology of cancer cells ^[23]. Expression and activity of different channel types mark and regulate specific stages of cancer establishment and progression ^[24]. Since more attention is recently paid on discovery of anticancer drugs that act as ion channels modulators ^[25], or blockers ^[20], the propafenone became good lead for design of novel antineoplastics ^[17, 26-27].

Previous SAR and QSAR studies of propafenone derivatives have selected the ethers, carbonyl and benzyl groups as well as the substitution pattern at the nitrogen atom (Figure 1) as determinants for pharmacological activity of the propafenone and its derivatives ^[18, 28].

Because of the previous finding that ether group of the propafenone derivatives is very important for their anticancer activity ^[18, 28] the aim of our

research work was to develop chalcones with hydroxyl group at the corresponding position (Scheme1), as compounds with potentially enhanced anticancer activity.

Expression and activity of different channel types mark and regulate specific stages of cancer progression in the cancer cells. New findings indicated that inner pore of the ion channels is formed from different aromatic and nonpolar aliphatic aminoacid residues ^[20-25]. Since benzyl moiety of the propafenone derivatives is also very important for their antineoplastic activity ^[18, 28] the hydrogen atom of the benzyl moiety of propafenone and chalcone was substituted with methyl-, trifluoromethyl-, fluoro-, and chloro- substituents (Scheme1). All these groups are lipophilic with different electronic and steric effects. These new substituents cause significant changes of lipophilicity and stereoelectronic properties of the benzyl moiety. Therefore, the substitution of H-atom by -F, -Cl atoms or -CH₃, -CF₃ atomic groups greatly change the conformational preferences of the chalcone and propafenone derivatives. These structural modifications could result in formation of stronger intermolecular bonds of the benzyl moiety of the chalcone/propafenone derivatives with hydrophobic aminoacid residues in the inner pore of the ion channels and enhanced anticancer activities. The changes in the ion channels activities caused by the chalcone/propafenone derivatives could have beneficial effect on anticancer activity of the other antineoplastics.

Also, these structural modifications of the chalcone molecules result in changes of lipophilicity and electron density on the double bond in ketovinyl

moiety and therefore have influence on the reaction with –SH groups of biological activates proteins. Introduction of electron donating groups(such as -CH₃) in the *ortho* or *para* position in the benzyl moiety increase electron density of carbon atoms in the double bonds that result in decrease of reactivity and activity of the compounds. But, introduction of electron withdrawing groups (such as -F, -Cl and –CF₃) in the *ortho* or *para* position in the benzyl moiety decrease electron density carbon atoms in the double bonds that increase reactivity and activity of the compounds.

So far, modifications of propafenone structure were performed on amino and ether moiety of the propafenone. These changes have an influence on lipophilicity and ionization of the compounds [26-28]. Since recent studies of ion channel blockers pointed on importance of the hydrophobic interactions between the ligand and the ion channel inside the pore [24], our synthetic route was focused on modification of the benzyl moiety of propafenone and its intermediary's chalcones.

Cytotoxic activities of twelve synthesized chalcone and propafenone derivatives were assayed against HeLa, Fem-X, K562, MCF-7, PC-3 and LS174 cancer cell lines. The QSAR studies of the examined chalcones and propafenone analogs have selected molecular descriptors and pharmacophores of the compounds responsible for their anticancer activities.

2. Results and Discussion

In this paper, the synthesis, anticancer activity of twelve 1,3-diphenylpropan-1-one derivatives as well as 2D and 3D QSAR studies aimed to rationalize

structural characteristics needed for significant potency, are reported. The set consist of six chalcones and six propafenone derivatives and their anticancer activities were evaluated toward six human tumor cell lines. The synthetic route and structures of proposed chalcones and propafenone derivatives are given in Scheme 1. Six simple 2'-hydroxychalcones bearing mono substituent in their ring B (methyl-, chloro-, fluoro- and trifluoromethyl-) were synthesized by *Claisen-Schmidt* method^[29] and evaluated for their anticancer *in vitro* activity. Due to the rapid development of tumor cells resistance to antiproliferative agents, it is vital to discover novel scaffold for the design and synthesis of the new low-molecular antiproliferative agents to help in the battle against tumor cell lines. These compounds, except 1a, are known in the literature, but their antiproliferative activity has not been investigated.

Since recent studies of ion channel blockers pointed on importance of the hydrophobic interactions between the ligand and the ion channel inside the pore^[24], our synthetic route was focused on modification of the benzyl moiety of propafenone introducing of trifluoromethyl, fluoro, chloro- or methyl groups in the *ortho* or *para* position.

2.1. Synthesis of chalcones and propafenone derivatives

Synthesis of the chalcones and novel propafenone derivatives is shown in the Scheme 1. The proposed derivatives were synthesized in five steps and their structures have been verified by IR, ¹H-NMR, ¹³C-NMR, ESI-MS and HRMS spectroscopy. The first step in the synthetic route consisted of the condensation of 2-hydroxy acetophenone with *ortho* or *para* mono substituted benzaldehydes

in basic conditions (10% aqueous NaOH) to give α,β -unsaturated ketones (chalcones, Scheme 1). The use of catalytic hydrogenation with a 5% Pd/C and careful monitoring of the H₂-consumption resulted in the formation of the saturated ketone structures (*ortho*-hydroxyphenones, 2a-f). The addition of phenolic nucleophiles to (\pm) epichlorohydrin in basic media led to the formation of aryloxyepoxipropane derivatives (3a-f) which were subjected to the aminolysis with propylamine to give the aryloxypropanolamine derivatives (amines). The formation of the hydrochlorides is performed by dissolving the amine in dry diethyl ether and adding 1M HCl solution in dry diethyl ether. The white precipitate of hydrochloride was filtered off and purified via crystallization (Scheme 1).

2.2. Cytotoxic studies

The antiproliferative activity of all given compounds was tested against six tumor cell lines: human cervical carcinoma (HeLa cells), human melanoma (Fem-x), human prostate cancer (PC-3), human breast cancer (MCF-7), human colon carcinoma (LS174 cells) and human chronic myelogenous leukemia (K562 cells). All compounds were also screened for cytotoxic activity against normal human peripheral blood mononuclear cells (PBMC) non-stimulated and stimulated with phytohaemagglutinin (PHA).

All compounds exerted a dose dependent antiproliferative action at micromolar concentrations toward investigated tumor cell lines, detected by MTT test. The results are given in Table 1. All compounds showed activity to all six cell lines, but HeLa, Fem-X and K562 cells were generally the most susceptible ones

with IC₅₀ values similar to cisplatin for some derivatives e.g. 5d, 1c, 5a. Cisplatin was used as positive control.

In order to investigate antiproliferative activity, the synthesized compounds were divided in two groups: 1) propafenone derivatives and 2) intermediate chalkones. Propafenone derivatives show better efficacy in inhibition of cancer cell proliferation (Table 1). According to results in Table 1, it is possible to make comparative efficacy ranking of derivatives on certain human cancer cell lines.

HeLA: 5d > 5a > 5b > 5c = 5e > 5f

Fem X: 5d > 5b > 5e > 5f > 5a > 5c

K562: 5d > 5b ~ 5a > 5f > 5e > 5c

MCF-7: 5a > 5c ~ 5d > 5b > 5f ~ 5e

PC-3: 5d > 5b > 5a > 5f > 5e > 5c

LS174: 5d > 5a ~ 5b > 5f > 5e > 5c

Ortho-substituted derivatives show better efficacy than *para*-substituted analogs and the most potent is 5d derivative. Introduction of electronegative, lipophilic chloro group in *ortho* position of benzyl moiety contributes better efficacy of this derivative compared to other synthesized compounds on five of six cancer cell lines. In our previous studies³⁰ we have demonstrated that propafenone derivatives with substituted terminal benzene ring (benzyl moiety) interact with ion channels and show better selectivity compared to *lead* molecule (propafenone). Those effects are confirmed in presence of selective ion channel blockers. *Para*-substituted derivatives showed better potassium channel selectivity, while the effects of *ortho*-substituted derivatives were not antagonized by potassium channel blockers.

Ortho-substituted derivatives (5d and 5a) showed selective effect on calcium channels. *In vitro* studies with 5d derivative on isolated rat aorta (unpublished results) showed that effect of 5d at concentrations lower than 10 μ M could be antagonized by channel blocker, which means that the effect is not selective. This fact may support our hypothesis that 5d derivative in lower concentration takes effect as a nonselective ion channel blocker. For that reason, this derivative is more potent than others, because cancer cells express various sub/types of channels depending on cell cycle phase.

Compound 5d showed the best activity on HeLa cell culture line (3 μ mol/l). HeLa cell line includes calcium permeability channels with nonselective permeability to potassium and other monovalent ions. Those channels are not voltage-dependent and show the characteristics of receptors channels [20, 24-25]. It can be assumed that 5d derivative exerts its antiproliferative effect by disrupting calcium homeostasis affected by potassium and calcium channels.

In vitro [30] and *in silico* studies (unpublished results) showed potential potassium blocker activity of *ortho*-fluorinated (5c) derivative. However, 5c derivative shows three to six times less effect than 5d derivative. There is no difference in effects of this derivative on normal and cancer cells (Table 2). Ion channels in cancerous cells differ from channels in normal cells. In this case, electronegativity of fluorine adversely affects the interactions of terminal benzene ring with channel aminoacids residues in cancerous cells. The exception is MCF-7 breast cancer line. The efficacy of 5d derivative is less than 5a, but almost equal as 5c. Those cells express calcium and BK_{Ca} channels [20, 24]. *In vitro* studies on rat aorta

showed better calcium channel selectivity of 5a derivate in comparison to other five derivates. Consequently, its activity on MCF-7 cell line is expected. Activity, as well as selectivity of investigated chalkones are less compared to propafenone derivates, due to chalkones non specific effect. According to literature data, activity of chalkones on HeLa, PC-3 and MCF-7 cell lines (in concentration range from nmol/l to mmol/l) depends on their structure^[4]. Test results show satisfactory anticancer activity of chalkones in concentration range 9-70 μ mol/l. This activity is lower or equivalent to activity described in literature, due to simple chemical structure of synthesized chalkones. It would mean that keto-vinyl group and its substituents are essential for anticancer activity. The efficacy of chalkones on all cell culture lines are approximate, which confirms chalkones non specific mechanism of action. Activity ranking follows electronegativity of substituents in the benzyl moiety.

HeLA: 1c > 1d > 1b ~ 1a > 1f > 1e

Fem X: 1c > 1d = 1a > 1e = 1f ~ 1b

K562: 1c > 1a > 1d > 1e ~ 1f ~ 1b

MCF-7: 1c > 1a > 1e > 1d > 1f > 1b

PC-3: 1b > 1d ~ 1c > 1f > 1e > 1a

LS174: 1c > 1a > 1d > 1e > 5f > 1b

Electropositive carbon atoms in double bond are more reactive to nucleophilic -SH groups of aminoacid residues with which chalkones react^[4].

The most potent chalkones compounds are 1OF (from 4.8 ± 0.6 on K562 to 21.6 ± 3.5 on PC-3 cell line) and 1OCl (from 9.8 ± 1.4 on K562 to 32.2 ± 1.2 on

LS174 cell line). The selectivity of chalcones derivatives is less compared to propafenone derivatives. Selectivity index for 1OF derivate is 3.67 on MCF-7 cell line, while is 0.81 on PC-3 cell line. 1CF3 derivate showed better selectivity (SI values from 4.55 on K562 to 1.04 on PC-3 cell line).

2.3. QSAR studies

The 2D-QSAR and 3D-QSAR studies were performed on twelve synthesized chalcone and propafenone derivatives (Scheme 1) with cytotoxic activities (Table 1) against six cancer cell lines (HeLa, Fem-X, K562, MCF-7, PC-3, and LS174).

The constitutional, geometrical, physico-chemical and electronic descriptors of the optimised molecular models were used as independent variables, while negative logarithm of cytotoxic activities ($pIC_{50} = (\log 1/IC_{50})$) were used as dependent variables for the QSAR studies. The PLS regression has been applied for selection of the most relevant molecular descriptors and QSAR models building.

The applied PLS methodology has selected sets of significant descriptors during development of each QSAR model. Overfitting of the QSAR models is avoided by two parallel procedures. First, during the QSAR modelling the RMSE for training and test set were monitored. The optimal QSAR models were selected when RMSEP of test set begins to increase while RMSEE of training set continues to decrease. Second, the formed QSAR models with different number of selected significant descriptors were compared and optimal one is chosen by comparing R^2 , Q^2 , RMSEE, $R^2_{Obs vs. Pred}$, and RMSEP.

Optimal 2D-QSAR models for each cell line (HeLa, Fem-X, K562, MCF-7, PC-3 and LS174) were selected by use of statistical parameters such as: R^2 , F ratio, P-value, RMSEE of the training set, the leave-one-out cross-validation parameter (Q^2), and external validation test set (Fig. 2) ($R^2_{\text{Obs vs. Pred}}$ and RMSEP (Tables 3-8).

The 2D-QSAR (HeLa) model relating five variables (HOMO, BIC4, and RDF145s), with one significant component ($A=1$), R^2 : 0.824, $Q^2(Y)$: 0.772, F ratio: 15.240, P-value: 0.001, RMSEE: 0.103, and RMSEP: 0.179 (Table 3), was formed.

The 2D-QSAR (Fem-X) model relating two variables (Mor08u and Mor27i), with one significant component ($A=1$), R^2 : 0.647, $Q^2(Y)$: 0.585, F ratio: 6.340, P-value: 0.019, RMSEE: 0.144, and RMSEP: 0.622 (Table 4), was created.

The 2D-QSAR (K562) model relating two variables (Mor06e and CMC-50), with one significant component ($A=1$), R^2 : 0.639, $Q^2(Y)$: 0.587, F ratio: 6.394, P-value: 0.018, RMSEE: 0.155, and RMSEP: 0.232 (Table 5), was selected.

The 2D-QSAR (MCF-7) model relating two variables (Eig02_AEA(dm), and H5s), with one significant component ($A=1$), R^2 : 0.822, $Q^2(Y)$: 0.812, F ratio: 19.4464, P-value: 0.0005, RMSEE: 0.071, and RMSEP: 0.124 (Table 6), was obtained.

The 2D-QSAR (PC-3) model relating two variables (Mor32s and G(O..Cl)), with one significant component ($A=1$), R^2 : 0.851, $Q^2(Y)$: 0.591, F ratio: 6.513, P-value: 0.017, RMSEE: 0.055, and RMSEP: 0.214 (Table 7), was formed.

The 2D-QSAR (LS174) model relating three variables (RDF04s, G1e, and G2u), with one significant component ($A=1$), R^2 : 0.609, $Q^2(Y)$: 0.555, F ratio: 5.608, P-value: 0.026, RMSEE: 0.133, and RMSEP: 0.266 (Table 8), was created.

In order to investigate the statistical significance of the $R^2(Y)$ and $Q^2(Y)$ and to test the model for overfitting due to the chance correlation the response permutation test (Y scrambling) is applied for all 2D-QSAR models [43, 45]. The $R^2(Y)$ – intercepts were less than 0.4 while the $Q^2(Y)$ -intercepts were less than 0.05 [43, 45] for the six developed 2D-QSAR models.

The 3D-QSAR studies of the cytotoxic activities of the chalcones and propafenone derivatives against six cancer cell lines (HeLa, Fem-X, K562, MCF-7, PC-3 and LS174) were started from computing highly relevant MIF-3D maps of interaction energies between the examined molecule and four chemical probes (DRY, O, N1 and TIP). These maps are encoded into GRIND and GRIND2 descriptors and compressed into new types of variables- with the intensity of the field at a node and the mutual node–node distances between the chosen nodes as a scoring function. The obtained variables create matrix of descriptors that were used for development of 3D-QSAR models by use of the PLS regression.

Quality of the obtained 3D-QSAR models was examined by use of the regression factor R^2 , the leave-one-out cross-validation parameter (Q^2), RMSEE of the training set, RMSEP of the test set, and $R^2_{\text{Obs vs. Pred}}$ of the test set (Fig. 2) (Tables 3-8).

The 3D-QSAR (HeLa) model with three significant components ($A=3$), R^2 : 0.97, $Q^2(Y)$: 0.75, RMSEE: 0.054, and RMSEP: 0.232 was created. The variables v366: DRY-N1, v301: DRY-O, and v568: O-TIP are positively correlated with the activity, while V155/v160: N1-N1 variables are negatively correlated with activity against HeLa cells.

The propafenone derivatives with substituent at *ortho* position of the benzyl moiety (5d, 5a, and 5b) were the most potent against HeLa cells. The strongest positive influences on cytotoxic activity of propafenone derivatives against HeLa cells were determined for O-TIP descriptors (v565, v566, v568), created between H-bond donating hydroxyl/or amino group and topological area at positions C4 and C5 of the benzyl group (Fig. 3A,3B); O-DRY descriptor (v301) formed between H-bond donating hydroxyl/or amino group and hydrophobic area of the benzyl moiety (Fig 3A, 3B); and N1-DRY descriptor (v366) created between H-bond accepting oxygen of hydroxyl group and hydrophobic area of the benzyl moiety (Figure 3A). The strongest negative influence on cytotoxic activity of propafenone derivatives against HeLa cells was determined for N1-N1 descriptors (v155/v160) created between H-bond accepting carbonyl and ether groups (Fig. 3B). Finally is concluded that the interactions between hydroxyl/or amino group with topological and hydrophobic regions of the benzyl moiety are responsible for stronger anticancer activity of the propafenone derivatives, while specific relations between H-bond accepting carbonyl and ether groups are able to decrease cytotoxic activity of the propafenone derivatives against HeLa cell lines.

The 3D-pharmacophore (HeLa) study indicated that further modification of the most active 5d propafenone derivative should start with substitution with bulk and hydrophobic substituents at the positions C4 or C5 of the benzyl moiety (O-TIP: v565, v566, v568; O-DRY: v301; N1-DRY: v366).

The 3D-QSAR (Fem-X) model with four significant components ($A=4$), R^2 : 0.98, $Q^2(Y)$: 0.58, RMSEE: 0.056, and RMSEP: 0.265 was developed. The variables v252: TIP-TIP, v367: DRY-N1, and v631: N1-TYP are positively correlated with the activity, while v164: N1-N1 variable is negatively correlated with activity against Fem-X cells.

The 5d, 5b, 1c, and 5e derivatives were the most potent against Fem-X cells. The strongest positive influences on cytotoxic activity of propafenone derivatives against Fem-X cells were observed for N1-TIP descriptor (v631), created between H-bond accepting carbonyl group and topological area of aliphatic chain at the nitrogen atom (Fig. 4A); N1-DRY descriptor (v367) formed between H-bond accepting carbonyl group and hydrophobic area of aliphatic chain at the nitrogen atom (Fig. 4A); and TIP-TIP variable (v252) created between position 4 of the benzyl moiety and propylamino moiety (Fig. 4A). The strongest negative influence on cytotoxic activity of the propafenone derivatives against Fem-X cells was determined for N1-N1 descriptors (v164) created between H-bond accepting nitrogen atom and fluorine substituent in the benzyl moiety (Fig. 4B). Finally is concluded that the specific interactions between carbonyl group with topological and hydrophobic regions of the aliphatic chain at the nitrogen atom are responsible for stronger anticancer activity of the propafenone derivatives, while

specific relations between H-bond accepting nitrogen atom and fluorine substituent in the benzyl moiety can attenuate cytotoxic activity of the propafenone derivatives against Fem-X cell lines (Fig. 4). The 3D-pharmacophore (Fem-X) study indicated that benzyl moiety at position C4 and aliphatic chain at the nitrogen atom of the propafenone molecule should be modified with bulk and hydrophobic groups (N1-TIP: v631, N1-DRY: v367, TIP-TIP: v252), Also, substituents with very strong electronegativity, such as fluorine, should be avoided (N1-N1: v164).

The 3D-QSAR (K562) model with two significant components ($A=2$), R^2 : 0.93, $Q^2(Y)$: 0.62, RMSEE: 0.052, and RMSEP: 0.288 was generated. The variables v633: N1-TIP, v532: O-TIP, and v252: TIP-TIP are positively correlated with the activity, while v164: N1-N1, v240: TIP-TIP, v265: DRY-O, and v425: DRY-TIP variables are negatively correlated with activity against K562 cells.

The 1c, 5d, 5b, 5a, and 1a compounds were the most potent against K562 cells. The strongest positive influences on K562 anticancer activity of the agents were determined for TIP-TIP descriptor (v252) created between benzyl moiety and topological area of aliphatic chain at the nitrogen atom (Fig. 5A); O-TIP descriptor (v532) created between H-bond donating hydroxyl group and topological area at *meta* position C4' (chalcone derivatives)/or aliphatic chain at the nitrogen atom (propafenone derivatives) (Fig. 5A, 5B, 5C); and N1-TIP descriptor (v633) created between H-bond accepting nitrogen atom and topological area of the benzyl moiety of the propafenone derivatives (Fig. 5A). The strongest negative influence on cytotoxic activity of the compounds against

K562 cells were determined for: N1-N1 descriptor (v164) created between H-bond accepting hydroxyl group and fluorine substituent (Fig. 5C); TIP-TIP variable (v240) formed between two benzene rings (positions C4 and C4') (Fig. 5B, 5C), and DRY-TIP descriptor (v425) created between two benzene rings or between benzene ring and aliphatic chain at the nitrogen atom (Fig. 5A and 5B). From this results is concluded that the specific interactions of the aliphatic chain at the nitrogen atom with benzyl moiety and with hydroxyl group are mainly responsible for anticancer activity of the propafenone derivatives, while specific interactions between H-bond accepting hydroxyl group and fluorine substituent and between topological areas at positions C4 and C4' of the two benzene rings have negative influence on cytotoxic activity of the propafenone derivatives against K562 cells. According to the 3D-pharmacophore (K562) study further synthesis of the propafenone derivatives should start with substitution with a bulk group at position-C2 of the benzyl moiety (N1-TIP: v633), while positions C4 and C4' of the two benzene rings should be unsubstituted (TIP-TIP: v240, DRY-TIP: v425). Also, substituents with very strong electronegativity, such as fluorine, should be avoided (N1-N1: v164).

The most important positive impact on anticancer activity of chalcone derivatives is determined for interaction between H-bond donating hydroxyl group and topological area at C4' position of the same benzene ring (O-TIP: v532), while relations between H-bond accepting hydroxyl group and fluorine substituent (N1-N1: v164) together with interactions between two benzene rings (TIP-TIP: v240, DRY-TIP: v425) have negative influence on anticancer activity of the

chalcone derivatives against K562 cells. According to the 3D-pharmacophore (K562) study further synthesis of the chalcone derivatives should start with substitution at the positions C2 or C6 of the phenyl group with electronegative substituents (O-TIP: v532), while positions C4 and C4' of the two benzene rings should be unsubstituted (TIP-TIP: v240, DRY-TIP: v425).

The 3D-QSAR (MCF-7) model with two significant components ($A=2$), R^2 : 0.95, $Q^2(Y)$: 0.80, RMSEE: 0.030, and RMSEP: 0.314 was obtained. The variables v548: O-TIP, v30: DRY-DRY, and v439: DRY-TIP are positively correlated with the activity, while v143: N1-N1 variable is negatively correlated with activity against MCF-7 cells.

The chalcone and propafenone derivatives with $-F$ or $-CF_3$ substituent at *ortho* position (5c, 5a, 1c, and 1a) were the most potent against MCF-7 cells. The strongest positive influences on cytotoxic activity of compounds against MCF-7 cells were determined for TIP-DRY descriptor (v439) formed between topological area at positions 4' and 5' of the benzene ring and hydrophobic region of aliphatic chain at nitrogen atom (Fig. 6A); DRY-DRY descriptor (v30) created between hydrophobic area of the benzyl moiety and aliphatic chain at nitrogen atom (Fig. 6A); and O-TIP descriptors (v548) formed between H-bond donating hydroxyl group and topological area at positions C4' of the benzene ring and between H-bond donating hydroxyl (phenol) group and topological area of aliphatic chain at nitrogen atom (Fig. 6A, 6B). The strongest negative influence on cytotoxic activity of the compounds against MCF-7 cells was determined for N1-N1 descriptors (v143) created between H-bond accepting carbonyl and hydroxyl groups of the

chalcone derivatives (Fig. 6B). Finally is concluded that the interactions between aliphatic chain of the amino group with topological and hydrophobic regions of the benzene ring (especially C4' and C5' positions) are responsible for stronger anticancer activity of the propafenone derivatives against MCF-7 cell lines.

The 3D-pharmacophore (MCF-7) study indicated that further modification of the most active 5a/5c propafenone derivatives should start with substitution with bulk and hydrophobic substituents at the position C4' or C5' of the benzene ring (TIP-DRY: v439, DRY-DRY: v30, O-TIP: v548). The 3D-pharmacophore (MCF-7) study indicated that modification of the most active 1a/1c chalcone derivatives should start with substitution with bulk and hydrophobic groups at the position 4 or 5 of the B-benzene ring (O-TIP).

The 3D-QSAR (PC-3) model with two significant components ($A=2$), R^2 : 0.96, $Q^2(Y)$: 0.75, RMSEE: 0.018, and RMSEP: 0.219 was formed. The variables v36: DRY-DRY, v294: DRY-O, and v252: TIP-TIP are positively correlated with the activity, while v157: N1-N1 variable is negatively correlated with activity against PC-3 cells.

The chalcone and propafenone derivatives with $-Cl$ or $-CH_3$ substituent at *ortho* position (5d, 5b, 1d, and 1b) were the most potent against PC-3 cells. The strongest positive influences on cytotoxic activity of the propafenone and chalcone derivatives against PC-3 cells were determined for DRY-O descriptor (v294) formed between hydrophobic region of the benzyl moiety (B-benzene ring) and H-bond donating hydroxyl (phenol) group (Fig. 7A, 7B, 7C); TIP-TIP descriptor (v252) created between topological area at positions C4', C4, and C5

of the benzene rings and aliphatic chain at nitrogen atom (Fig. 7A, 7B); and DRY-DRY descriptor (v36) created between hydrophobic area of the benzyl moiety and aliphatic chain at nitrogen atom (Fig. 7A, 7B). The strongest negative influence on cytotoxic activity of the compounds against PC-3 cells was determined for N1-N1 descriptors (v157) created between H-bond accepting carbonyl and amino groups of the propafenone derivatives (Fig. 7A, 7B). Finally is concluded that the interactions between aliphatic chain of the amino group with topological and hydrophobic regions of the benzene ring (especially C4', C4 and C5 positions) are responsible for stronger anticancer activity of the propafenone derivatives against PC-3 cell lines.

The 3D-pharmacophore (PC-3) study indicated that further modification of the most active 5d/5b propafenone derivatives should start with substitution with bulk and hydrophobic groups at the position C4', C4 or C5 of the benzene rings (TIP-TIP: v252, DRY-DRY: v36), together with substitution with hydrophobic and electronegative group in aliphatic chain at nitrogen atom (TIP-TIP: v252, DRY-DRY: v36, DRY-O: v294). The 3D-pharmacophore (PC-3) study indicated that modification of the most active 1b/1d chalcone derivatives should begin with substitution with hydrophobic group in the B-benzene ring (DRY-O: v294).

The 3D-QSAR (LS174) model with three significant components ($A=3$), R^2 : 0.96, $Q^2(Y)$: 0.76, RMSEE: 0.057, and RMSEP: 0.177 was created. The variables v366: DRY-N1, and v632: N1-TIP are positively correlated with the activity, while v226: TIP-TIP variable is negatively correlated with activity against LS174 cells.

The 5d, 1c, 5a, 5b, and 5f derivatives were the most active against LS174 cells. The strongest positive influences on cytotoxic activity of the propafenone derivatives against LS174 cells were determined for DRY-N1 descriptor (v366) formed between hydrophobic region of the benzyl moiety and H-bond accepting hydroxyl group (Fig. 8A, 8B); and N1-TIP descriptors (v632) created between H-bond accepting carbonyl/or hydroxyl group and topological area at positions C5'/or C4 of the benzene rings (Fig. 8A, 8B). The strongest negative influence on cytotoxic activity of the compounds against LS174 cells was determined for TIP-TIP descriptors (v226) created between topological areas around hydroxyl group and positions C4' and C5' of the benzene ring of the propafenone derivatives (Fig. 8A, 8B). Finally is concluded that the interactions carbonyl/or hydroxyl group with topological and hydrophobic regions of the benzene rings (especially C5' and C4 positions) have influence on stronger anticancer activity, while topological relations between hydroxyl group and positions C4'/or C5' of the benzene ring of the propafenone derivatives have negative impact on their activity against LS174 cells.

The 3D-pharmacophore (LS174) study indicated that further modification of the most active 5d/5a propafenone derivatives should start with substitution with bulk and hydrophobic groups at the position C4 of the benzyl moiety (N1-TIP: v602, DRY-N1: v366, TIP-TIP: v226). Substitution of the positions C4' and C5' of the benzene ring of the propafenone derivatives should be avoided because of the unfavourable interaction (TIP-TIP: v226).

Predictive potentials of the developed 2D-QSAR models for each cell line (HeLa, Fem-X, K562, MCF-7, PC-3 and LS174) were compared with the corresponding 3D-QSAR models by use of R^2 , Q^2 , RMSEE, RMSEP and $R^2_{\text{Obs vs. Pred}}$ of the test set (Fig. 2) (Tables 3-8).

The obtained 3D-QSAR models for the anticancer activities on HeLa, Fem-X, K562, MCF-7, PC-3, and LS174 cell lines have expressed better statistical parameters (R^2 , Q^2 , RMSEE, RMSEP and $R^2_{\text{Obs vs. Pred}}$ of the test set) than the corresponding 2D-QSAR models (Tables 3-8).

The N1-TIP descriptors (v631-v633), created between H-bond accepting carbonyl/or hydroxyl group and topological area at positions C5'/or C4 of the benzene rings, have positive influence on activity against Fem-X, K562, and LS174 cell lines (Fig. 4, 5, 8). The TIP-TIP descriptor (v252), created between topological area at positions C4', C4, and C5 of the benzene rings and aliphatic chain at nitrogen atom, exert positive impact on anticancer activity on Fem-X, K562, and PC-3 cells (Fig. 4, 5, 7). The DRY-N1 descriptor (v366/v367), formed between hydrophobic region of the benzyl moiety and H-bond accepting hydroxyl group, have positive influence on activity against HeLa, Fem-X, and LS174 cell lines (Fig. 3, 4, 8). The O-TIP descriptors (v532, v548, v568), formed between H-bond donating hydroxyl group and topological area at positions C4' of the benzene ring and between H-bond donating hydroxyl (phenol) group and topological area of aliphatic chain at nitrogen atom, exert positive impact on anticancer activity on HeLa, K562, and MCF-7 cells (Fig. 3, 5, 6). The N1-N1 descriptors (v143-v164), created between two H-bond accepting groups, have

negative influence on activity against HeLa, Fem-X, K562, MCF-7, and PC-3 cell lines (Fig. 3-7). Generally, high level of similarity was observed for 3D-pharmacophores of the examined compounds responsible for HeLa, Fem-X, K562, and PC-3 anticancer activities.

3. Conclusion

Series of twelve chalcone and propafenone derivatives has been synthesized and evaluated for anticancer activities against HeLa, Fem-X, PC-3, MCF-7, LS174 and K562 cell lines.

The relationship between chemical structures of the synthesized compounds and their cytotoxic activities against the six cancer cell lines, were examined by 2D-QSAR and 3D-QSAR studies. The developed QSAR models have expressed good quality in activity prediction of the cross-validation and external validation test set compounds.

The performed QSAR studies of the chalcone and propafenone derivatives have selected molecular descriptors and pharmacophore features responsible for their antineoplastic activities against six cancer cell lines. Results of the 3D-QSAR studies were used for design of novel chalcones and propafenone derivatives with enhanced anticancer activity on the HeLa, Fem-X, PC-3, MCF-7, LS174 and K562 cells.

4. Material and methods

4.1. Chemistry

All solvents and reagents used are analytical grade having >98% purity. For the chemical synthesis and analysis of chalcones and propafenone derivatives the following compounds were used: 2-fluorobenzaldehyde, 4-fluorobenzaldehyde, 2-methylbenzaldehyde and 4-methylbenzaldehyde (Merck, Darmstadt, Germany), 2-trifluoromethylbenzaldehyde, 2-hydroxyacetophenone, 2-chlorobenzaldehyde, epichlorhydrine, propylamine (Sigma-Aldrich Inc., St. Louis, MO, USA), methanol, toluene, n-hexane, hydrochloride acid, sodium hydroxyde, ethanol (Sigma-Aldrich Inc., St. Louis, MO, USA). Melting points were determined on the Boetius PHMK 05 apparatus (VEB Wagetechnik Rapido, Radebeul, Germany) and are uncorrected. TLC was carried out using silica gel plates (TLC Silica gel 60 F₂₅₄ aluminium sheets, Merck Darmstadt, Germany) and the spots were visualized under UV light at 254 nm. Flash chromatography was performed for purification of the compounds on silica gel 60 (70-230 mesh ASTM) (Merck Darmstadt, Germany). The structure of each compound was confirmed by IR, NMR and LC-MS spectroscopy. The IR spectra were recorded on the Thermo Nicolet 6700 FT-IR spectrophotometer using ATR technique in the range 4000-600 cm⁻¹. The NMR spectra were recorded on the Varian Gemini 200 (¹H NMR spectra at 200 MHz and ¹³C NMR spectra at 50 MHz) for samples in deuterated chloroform. Chemical shifts are expressed in *ppm* using tetramethylsilane as the internal standard; coupling constants (*J*) are in Hz. Splitting patterns are described as singlet (s), doublet (d), triplet (t) multiplet (m) and broad signal (bs). The mass spectra of compounds were conducted on a TSQ Quantum Access MAX triple quadripole spectrometer (Thermo Fisher

Scientific) equipped with electrospray ionization (ESI) source operating in positive ion mode. Xcalibur software v 2.1.0.1139 (Thermo Fisher Scientific) was used for data acquisition and processing. The purity of the compounds was checked using HPLC (Agilent 1200 Series HPLC system, Agilent Technologies, Palo Alto, CA USA) and electrospray ionization-high resolution mass spectrometry (ESI/HRSM) were carried out on the Agilent 6210 time-of-flight LC/MS system (G1969A, Agilent Technology, Palo Alto, CA, United States). Agilent MassHunter Workstation software was used for data acquisition. Purity of the compounds was > 95%.

4.1.1. General procedure for the synthesis of chalcones

General methods for the preparation of chalcones involve Claisen-Schmidt condensation of appropriate 2-hydroxyacetophenones and benzaldehydes in presence of base (Scheme 1).

2-hydroxyacetophenone (0,012 mol) and substituted benzaldehyde (0,01 mol) are dissolved in 96 % ethanol (10 ml) with stirring. Solution of sodium hydroxide (10%, 20 g) in water was added in portions to give a blood-red solution that was stirred overnight during which chalcones, precipitated as the sodium salts. The solution/suspension was kept 24 h at 0 °C with occasional shaking, diluted with ice water and acidified with cold 1M HCl (pH about 3). The resulting yellow precipitate was filtered, washed with water (to neutral reaction to lacmus paper) and crude mixtures were purified by flash column chromatography with toluene as eluent. After removal of toluene under vacuum the crude products

precrySTALLIZED from ethanol. *Trans* isomers of propane moiety of chalcones were confirmed by the coupling constants of vinyl hydrogens (15-16 Hz).

1a (C₁₆H₁₁F₃O₂): (*E*)-1-(2-hydroxyphenyl)-3-(2-(trifluoromethyl) phenyl) prop-2-en-1-one. The yellow solid was recrystallized from ethanol. Yield: 88.6%; Melting point 111-114° C. **IR (ATR) (cm⁻¹):** 3438.9 (-OH), 1645.1(-C=O), 1586.1 (ArC-C-), 1205.6 (ArC-OH), 1154.7(ArC-F); **¹H NMR data (δ, ppm):** 12.66 (s, 1H, -OH), 8.31 (d, 1H, *J*=15.72, b), 7.93-7.73 (m, 4H, ArH; 6', 4', 3, 5), 7.63-7.37 (m, 5H, a, ArH: 3', 5', 4, 6); **¹³C NMR data (δ, ppm):** 193.29; 163.70; 140.71; 136.76; 133.70; 132.15; 130.04; 129.78; 128.04; 126.43; 126.63; 126.32; 124.45; 119.77; 118.73; 118.97; **LC-MS: *m/z* =** 291.00 (M⁺-1), 145.08, 251.14, 271.02, 263.08, 289.12, 231.10; **HRMS:** Measured mass for [M-H]⁻ is 291.06321, calculated mass for C₁₆H₁₀F₃O₂ is 291.06384.

1b (C₁₆H₁₄O₂): (*E*)-1-(2-hydroxyphenyl)-3-*o*-tolylprop-2-en-1-one. The yellow solid was recrystallized from ethanol. Yield: 90.8%; Melting point 153-156° C. **IR (ATR) (cm⁻¹):** 3015.3 (-OH), 1636.5 (-C=O), 1575.5 (ArC-C-), 1258.2(ArC-OH); **¹H NMR data (δ, ppm):** 12.84 (s, 1H, -OH), 8.27 (d, 1H, *J*=15.60, b), 7.94 (dd, 1H, *J*₁=8.20, *J*₂=1.40, ArH 6'), 7.73-7.56 (m, 3H, a, ArH: 4', 6), 7.38-7.23 (m, 3H, ArH: 3, 4, 5), 7.05-7.690 (m, 2H, ArH: 3', 5'), 2.50 (s, 3H, -CH₃); **¹³C NMR data (δ, ppm):** 193.80; 163.65; 143.07; 138.65; 136.39; 133.63; 131.04; 130.66; 129.69; 126.54; 126.42; 121.19; 120.02; 118.86; 118.62; 19.81; **HRMS:** Measured mass for [M-H]⁻ is 237.09267, calculated mass for C₁₆H₁₃O₂ is 237.09210.

1c (C₁₅H₁₁FO₂): (*E*)-1-(2-hydroxyphenyl)-3-(2-fluorophenyl) prop-2-en-1-one. The yellow solid was recrystallized from ethanol. Yield: 83.3%; Melting point 82-

83° C. **IR (ATR) (cm⁻¹):** 3438.0 (-OH), 1642.9 (-C=O), 1576(ArC-C-), 1203.2 (ArC-OH), 1155.2 (ArC-F); **¹H NMR data (δ, ppm):** 12.77 (s, 1H, -OH), 8.04 (d, 1H, *J*=15.72, b), 7.94 (dd, 1H, *J*₁=8.14, *J*₂=1.68, ArH: 6'), 7.82 (d, 1H, *J*=15.73, a), 7.70 (td, 1H, *J*₁=7.58, *J*₂=1.69, ArH 4'), 7.55-7.36 (m, 2H, ArH: 5', 6), 7.26-6.91 (m, 4H, ArH: 3, 4, 5, 3'); **¹³C NMR data (δ, ppm):** 193.84; 164.45; 163.65; 159.37; 138.25; 136.54; 132.31; 132.15; 130.20; 130.15; 129.75; 124.63; 124.58; 122.94; 122.79; 119.97; 118.91; 118.64; 116.62; 116.18; **HRMS:** Measured mass for [M-H]⁻ is 241.06615, calculated mass for C₁₅H₁₀FO₂ is 241.06703.

1d (C₁₅H₁₁ClO₂): (*E*)-1-(2-hydroxyphenyl)-3-(2-chlorophenyl) prop-2-en-1-one. The yellow solid was recrystallized from ethanol. Yield: 82.5%; Melting point 50-53° C. **IR (ATR) (cm⁻¹):** 1637.8 (-C=O), 1574.3(ArC-C-), 1203.4(ArC-OH), 1019.9 (ArC-Cl); **¹H NMR data (δ, ppm):** 12.75 (s, 1H, -OH), 8.34 (d, 1H, *J*=15.17, b), 7.93 (dd, 1H, *J*₁=7.76, *J*₂=1.68, ArH 6'), 7.79-7.74 (m, 1H, ArH 4'), 7.67 (d, 1H, *J*=15.73, a), 7.55-7.42 (m, 2H, ArH: 3, 6), 7.39-7.26 (m, 2H, ArH: 4, 5), 7.05-6.90 (m, 2H, ArH: 3', 5'); **¹³C NMR data (δ, ppm):** 193.49; 163.63; 141.14; 136.59; 135.72; 132.88; 131.53; 130.40; 129.71; 127.89; 127.13; 122.65; 119.84; 118.91; 118.66; **HRMS:** Measured mass for [M-H]⁻ is 257.03784, calculated mass for C₁₅H₁₀ClO₂ is 257.03748.

1e (C₁₅H₁₁FO₂): (*E*)-1-(2-hydroxyphenyl)-3-(4-fluorophenyl) prop-2-en-1-one. The yellow solid was recrystallized from ethanol. Yield: 56.0%; Melting point 84-88° C. **IR (ATR) (cm⁻¹):** 1635.7 (-C=O), 1570.6 (ArC-C-), 1203.2 (ArC-OH), 1155.3(ArC-F); **¹H NMR data (δ, ppm):** 12.79 (s, 1H, -OH), 7.94 (dd, 1H, *J*₁=7.80,

$J_2=1.68$, ArH 6'), 7.93 (d, 1H, $J=15.45$, b), 7.70-7.46 (m, 4H, a, ArH: 2, 6, 4'), 7.26-6.91 (m, 4H, ArH: 3, 5, 3', 5'); **^{13}C NMR data** (δ , ppm): 193.56; 166.82; 163.63; 161.79; 144.15; 136.48; 130.91; 130.71; 130.53; 129.60; 119.95; 119.84; 119.81; 118.88; 118.68; 116.47; 116.04; **HRMS**: Measured mass for $[\text{M}-\text{H}]^-$ is 241.06636, calculated mass for $\text{C}_{15}\text{H}_{10}\text{FO}_2$ is 241.06703.

1f ($\text{C}_{16}\text{H}_{14}\text{O}_2$): (*E*)-1-(2-hydroxyphenyl)-3-*p*-tolylprop-2-en-1-one. The yellow solid was recrystallized from ethanol. Yield: 93.8%; Melting point 117-118° C. **IR (ATR) (cm^{-1})**: 1634.1 ($-\text{C}=\text{O}$), 1563.3 (ArC-C-), 1199.2 (ArC-OH); **^1H NMR data** (δ , ppm): 12.86 (s, 1H, -OH), 7.95-7.87 (m, 2H, ArH: 4', 6'), 7.65-7.45 (m, 4H, a, b, ArH: 4, 6), 7.26 (d, 2H, $J=7.8$, ArH: 3, 5), 7.05-6.90 (m, 2H, ArH: 3', 5'), 2.40 (s, 3H, $-\text{CH}_3$); **^{13}C NMR data** (δ , ppm): 193.84; 163.61; 145.59; 141.60; 136.27; 131.91; 129.80; 129.62; 128.73; 120.08; 119.06; 118.79; 118.60; 21.52; **HRMS**: Measured mass for $[\text{M}-\text{H}]^-$ is 237.09312, calculated mass for $\text{C}_{16}\text{H}_{13}\text{O}_2$ is 237.09210.

4.1.2. General procedure for the synthesis of ortho-hydroxyphenones (2a-f)

A solution of the chalcones in the methanol (3.39 mmol/150ml) was transferred into a flask containing 5% Pd/C (200 mg) dispersed into methanol (10 ml) and the flask connected with a Parr apparatus filled with H_2 . The hydrogenation was carried at 1 atm of H_2 for 70 min, then the flask was purged with N_2 and the catalyst was filtered off on Celite. The solvent was evaporated and products 2a-f was isolated by column chromatography on silica gel (eluent toluene/ hexane 1/1) (Scheme 1).

2a (C₁₆H₁₃F₃O₂): 1-(2-hydroxy-phenyl)-3-(2-trifluoromethyl-phenyl)-propan-1-one. The white solid was recrystallized from methanol. Yield: 98.6%; **IR (ATR) (cm⁻¹):** 1638.9 (-C=O); **¹H NMR data (δ, ppm):** 12.27 (s, 1H, -OH), 7.73 (dd, 1H, *J*₁=7.80, *J*₂=1.60, ArH 6'), 7.67 (d, 1H, *J*=7.80, ArH 3), 7.53-7.25 (m, 4H, ArH: 4, 5, 6, 4'), 7.01 (dd, 1H, *J*₁=8.40, *J*₂=1.00, ArH 5'), 6.91-6.83 (m, 1H, ArH 3'), 3.37-3.19 (m, 4H, a, b); **¹³C NMR data (δ, ppm):** 204.74; 162.45; 139.49; 136.45; 132.04; 131.24; 129.71; 127.29; 126.52; 126.21; 126.11; 121.85; 119.11; 118.95; 118.53; 40.02; 26.84;

2b (C₁₆H₁₆O₂): 1-(2-hydroxy-phenyl)-3-*o*-tolyl-propan-1-one: The white solid was recrystallized from methanol. Yield: 90.6%; **IR (ATR) (cm⁻¹):** 1630.4 (-C=O); **¹H NMR data (δ, ppm):** 12.32 (s, 1H, -OH), 7.76 (dd, 1H, *J*₁=7.80, *J*₂=1.68, ArH 6'), 7.51-7.42 (m, 1H, ArH 4'), 7.24-6.91 (m, 5H, ArH: 3, 4, 5, 6, 5'), 6.88 (d, 1H, *J*=7.40, ArH 3'), 3.32-3.24 (m, 2H, a), 3.08-3.01 (m, 2H, b), 2.35 (s, 3H, -CH₃); **¹³C NMR data (δ, ppm):** 205.58; 162.48; 138.80; 136.37; 135.96; 130.42; 129.78; 128.65; 126.49; 126.23; 119.24; 118.91; 118.57; 38.67; 27.35; 19.28;

2c (C₁₅H₁₃FO₂): 1-(2-hydroxy-phenyl)-3-(2-fluoro-phenyl)-propan-1-one. The white solid was recrystallized from methanol. Yield: 93.3%; **IR (ATR) (cm⁻¹):** 1634.5 (-C=O); **¹H NMR data (δ, ppm):** 12.26 (s, 1H, -OH), 7.77-7.72 (m, 1H, ArH 6'), 7.55-7.39 (m, 1H, ArH 4'), 7.29-6.83 (m, 6H, ArH: 3, 4, 5, 6, 3', 5'), 3.37-3.29 (m, 2H, a), 3.13 (t, 2H, *J*=7.8, b); **¹³C NMR data (δ, ppm):** 205.18; 162.44; 138.29; 136.37; 132.15; 130.91; 129.82; 128.25; 127.34; 124.21; 122.96; 119.22; 118.95; 118.53; 115.58, 115.14, 38.42; 23.84;

2d ($\text{C}_{15}\text{H}_{13}\text{ClO}_2$): 1-(2-hydroxy-phenyl)-3-(2-chloro-phenyl)-propan-1-one. The white solid was recrystallized from methanol. Yield: 92.5%; **IR (ATR) (cm^{-1}):** 1638.4 ($-\text{C}=\text{O}$); **^1H NMR data (δ , ppm):** 12.28 (s, 1H, -OH), 7.78 (dd, 1H, $J_1=7.86$, $J_2=1.68$, ArH 6'), 7.50-7.16 (m, 5H, ArH: 3, 4, 5, 6, 4'), 7.01 (d, 1H, $J=8.43$, ArH 5'), 6.91-6.83 (m, 1H, ArH 3'), 3.38-3.30 (m, 2H, a), 3.21-3.13 (m, 2H, b); **^{13}C NMR data (δ , ppm):** 205.22; 162.45; 138.27; 136.39; 133.93; 130.77; 129.87; 129.64; 127.94; 127.03; 119.24; 118.95; 118.53; 38.04; 28.20;

2e ($\text{C}_{15}\text{H}_{13}\text{FO}_2$): 1-(2-hydroxy-phenyl)-3-(4-fluoro-phenyl)-propan-1-one. The white solid was recrystallized from methanol. Yield: 96.0%; **IR (ATR) (cm^{-1}):** 1640.2 ($-\text{C}=\text{O}$); **^1H NMR data (δ , ppm):** 12.27 (s, 1H, -OH), 7.76 (dd, 1H, $J_1=7.87$, $J_2=1.69$, ArH 6'), 7.51-7.42 (m, 1H, ArH 4'), 7.25-7.17 (m, 2H, ArH 2, 6) 7.04-6.84 (m, 1H, ArH: 3, 5, 3', 5'), 3.35 (t, 2H, $J=7.87$, a), 3.08 (t, 2H, $J=7.86$, b); **^{13}C NMR data (δ , ppm):** 205.16; 163.92; 162.45, 159.06, 136.43; 129.89; 129.75; 119.22; 118.95; 118.59; 115.55, 115.13, 39.99; 29.08;

2f ($\text{C}_{16}\text{H}_{16}\text{O}_2$): 1-(2-hydroxy-phenyl)-3-*p*-tolyl-propan-1-one. The white solid was recrystallized from methanol. Yield: 93.8%; **IR (ATR) (cm^{-1}):** 1630.4 ($-\text{C}=\text{O}$); **^1H NMR data (δ , ppm):** 12.31 (s, 1H, -OH), 7.76 (dd, 1H, $J_1=7.86$, $J_2=1.69$, ArH 6'), 7.50-7.41 (m, 1H, ArH 4'), 7.13 (s, 4H, ArH: 2, 3, 5, 6) 7.00 (dd, 1H, $J_1=8.42$, $J_2=1.12$ ArH 5'), 6.91 (t, 1H, $J=7.86$, ArH 3'), 3.35-3.27 (m, 2H, a), 3.06-2.99 (t, 2H, $J=7.80$, b), 2.32 (s, 3H, $-\text{CH}_3$); **^{13}C NMR data (δ , ppm):** 205.56; 162.50; 137.63, 136.32; 135.86; 129.84; 129.29, 128.27, 119.30; 118.91; 118.57, 40.17; 29.59, 20.58;

4.1.3. General procedure for the synthesis of epoxides (3a-f)

Ortho-hydroxyphenone (45.78 mmol) was dissolved in 100 ml of epichlorohydrine and 60 mmol of powdered NaOH was added. The reaction mixture was refluxed for 7 h, cooled on room temperature and evaporated to dryness. The resulting orange oil was dissolved in diethyl ether and extracted several times with water. The organic layer was dried over Na₂SO₄ and the solvent removed under reduced pressure. The resulting yellow oil was put into the next reaction step without further purification and characterization (Scheme 1).

4.1.4. General procedure for the synthesis of amines (4a-4f)

Epoxide 3a-f (17 mmol) was dissolved in 30 ml of *n*-propyl amine and refluxed for 6 h until the reaction was completed (TLC control). The solvent was evaporated to dryness under reduced pressure and the brown oily residue was purified via column chromatography (silica gel, CH₂Cl₂/methanol/conc.NH₃ 200/10/1.5) (Scheme 1).

4.1.5. General procedure for the synthesis of hydrochlorides (5a-5f)

Formation of the hydrochlorides was carried out by dissolving the amines in dry diethyl ether and adding a 1M solution of HCl in diethyl ether. The resulting precipitate was filtered off and purified via crystallization in mixture acetone/methanol 1:1 to give the white powder (Scheme 1).

5a (C₂₂H₂₇F₃ClNO₃): 3-(2-trifluoromethyl-phenyl)-1-[2-(2-hydroxy-3-propylamino-propoxy)-phenyl]-propan-1-one hydrochloride salt. The white solid was recrystallized from mixture acetone/methanol 1:1. Yield: 63.8%; Melting point: 157.4-158.6 °C IR (ATR) (cm⁻¹): 3385.9 (-OH), 2961.3 (-NH-), 1667.2 (-C=O),

1597.9 (ArC-C-); **¹H NMR data (δ, ppm):** 9.25 and 8.98 (bs 1H, -NH), 7.72 (dd, 1H, $J_1=7.80$, $J_2=1.60$, ArH 6'), 7.63 (d, 1H, $J=7.80$, ArH 3), 7.55-7.27 (m, 4H, ArH: 4, 5, 6, 4'), 7.04-6.96 (m, 2H ArH 3', 5'), 5.68 (bs, 1H, -OH), 4.25-4.11 (m, 2H, c), 3.32-3.20 (m, 6H a, b, e, f), 2.99-2.91 (m, 2H, f), 1.99-1.84 (m, 2H, g), 1.02 (t, 3H, $J=7.40$, h); **¹³C NMR data (δ, ppm):** 200.76; 157.24; 139.89; 134.38; 132.17; 131.22; 130.68, 126.65; 126.31; 126.07; 125.96, 121.24; 113.18; 71.32, 64.77, 51.44; 50.45, 43.83; 26.89, 19.27, 11.04; **LC-MS: m/z** = 410.10 (M^++1), 116.12, 392.18, 333.05, 98.11, 72.26, 173.00; **HRMS:** Measured mass for $[M-H]^-$ is 408.17790, calculated mass for $C_{22}H_{26}F_3NO_3 - H^+$ is 408.17920.

5b (**$C_{22}H_{30}ClNO_3$**): 3-(2-methyl-phenyl)-1-[2-(2-hydroxy-3-propylamino-propoxy)-phenyl]-propan-1-one hydrochloride salt. The white solid was recrystallized from mixture acetone/methanol 1:1. Yield: 70.8%; Melting point 104.9-106.7 °C. **IR (ATR) (cm^{-1}):** 2971.1(-NH-), 1663.4 (-C=O), 1597.1(ArC-C-); **¹H NMR data (δ, ppm):** 9.18 and 8.86 (bs 1H, -NH), 7.73 (dd, 1H, $J_1=7.80$, $J_2=1.80$, ArH 6'), 7.52-7.44 (m, 1H, ArH 4'), 7.13-6.99 (m, 6H, ArH: 3, 4, 5, 6, 3', 5'), 5.65 (bs, 1H, -OH), 4.63 (m, 1H, c), 4.20 (m, 2H, c, d), 3.28-2.87 (m, 8H, a, b, e, f), 2.32 (s, 3H, Ar-CH₃), 1.96-1.72 (m, 2H, g), 1.03-0.93 (m, 3H, h); **¹³C NMR data (δ, ppm):** 201.52; 157.15; 139.12; 136.01; 134.28; 130.29, 128.45; 126.85; 126.25; 121.21; 113.23; 71.25, 64.71, 51.13; 50.29, 42.55; 41.51, 27.46, 20.89, 19.32, 11.09; **LC-MS: m/z** = 356.20 (M^++1), 116.14, 338.20, 98.16, 72.27, 105.13, 279.16; **HRMS:** Measured mass for $[M+H]^+$ is 355.22061, calculated mass for $C_{22}H_{29}NO_3 + H^+$ is 356.22202.

5c ($\text{C}_{21}\text{H}_{27}\text{FCINO}_3$): 3-(2-fluoro-phenyl)-1-[2-(2-hydroxy-3-propylamino-propoxy)-phenyl]-propan-1-one hydrochloride salt. The white solid was recrystallized from mixture acetone/methanol 1:1. Yield: 73.8%; Melting point: 153.9-154.6 °C **IR (ATR) (cm^{-1}):** 2969.4 (-NH-), 1658.7 (-C=O), 1594.2 (ArC-C-); **^1H NMR data (δ , ppm):** 9.50 i 8.90 (bs 1H, -NH), 7.76 (dd, 1H, $J_1=7.80$, $J_2=1.60$, ArH 6'), 7.53-7.44 (m, 1H, ArH 4'), 7.26-6.96 (m, 6H, ArH; 3, 4, 5, 6, 3', 5'), 5.58 (bs, 1H, -OH), 4.60-4.57 (m, 1H, c), 4.20-4.18 (m, 2H, c', d), 3.35-3.26 (m, 3H, a, e), 3.07-2.99 (m, 5H, b, e, f), 2.04-1.93 (m, 2H, g), 1.05 (t, 3H, $J=7.20$, h); **^{13}C NMR data (δ , ppm):** 201.30; 160.3, 157.20; 134.52; 130.89, 128.09; 127.93; 126.49; 124.27, 121.32; 115.53; 115.07, 113.16, 71.43, 64.77, 51.56; 50.62, 42.02; 23.94, 19.36, 11.14; **LC-MS: m/z** = 360.10 (M^++1), 116.14, 342.19, 98.14, 283.06, 72.25, 109.08; **HRMS:** Measured mass for $[\text{M}+\text{H}]^+$ is 360.19695, calculated mass for $\text{C}_{21}\text{H}_{26}\text{FNO}_3+\text{H}^+$ is 360.19695

5d ($\text{C}_{21}\text{H}_{26}\text{ClNO}_3$): 3-(2-Chloro-phenyl)-1-[2-(2-hydroxy-3-propylamino-propoxy)-phenyl]-propan-1-one hydrochloride salt. The white solid was recrystallized from mixture acetone/methanol 1:1. Yield: 62.8%; Melting point: 145.8-146.9 °C **IR (ATR) (cm^{-1}):** 2934.7 (-NH-), 1659.2 (-C=O), 1593.5 (ArC-C-); **^1H NMR data (δ , ppm):** 8.89 (bs 1H, -NH), 7.79 (dd, 1H, $J_1=7.80$, $J_2=1.60$, ArH 6'), 7.57-7.48 (m, 1H, ArH 4'), 7.38-7.02 (m, 6H, ArH; 3, 4, 5, 6, 3', 5'), 4.53-4.43 (m, 1H, c), 4.27-4.10 (m, 2H, d, c), 3.54 (bs, 1H, -OH), 3.37-3.29 (m, 3H, a, e), 3.22-2.95 (m, 5H, b, e, f), 2.01-1.81 (m, 2H, g), 1.07 (t, 3H, $J=7.40$, h); **^{13}C NMR data (δ , ppm):** 201.32; 157.02; 138.27; 134.54, 133.66, 130.78; 130.35, 129.36; 128.38; 127.67, 126.91, 126.03; 121.13; 112.92, 71.28, 64.11, 51.00; 50.11,

41.30; 28.11, 19.03, 10.80; **LC-MS**: m/z = 376.10 ($M^+ + 1$), 116.13, 358.15, 98.12, 72.25, 299.05, 125.01; **HRMS**: Measured mass for $[M+H]^+$ is 376.16709, calculated mass for $C_{21}H_{26}FNO_3 + H^+$ is 376.16740.

5e (**$C_{21}H_{27}FCINO_3$**): 3-(4-fluoro-phenyl)-1-[2-(2-hydroxy-3-propylamino-propoxy)-phenyl]-propan-1-one hydrochloride salt. The white solid was recrystallized from mixture acetone/methanol 1:1. Yield: 66.3%; Melting point 138.9-140.7 °C; **IR (ATR) (cm^{-1})**: 2971.7 (-NH-), 1662.1 (-C=O), 1594.2 (ArC-C-); **1H NMR data (δ , ppm)**: 7.75 (dd, 1H, $J_1=7.80$, $J_2=1.60$, ArH 6'), 7.53-7.48 (m, 1H, ArH 4'), 7.23-6.93 (m, 6H, ArH: 2, 3, 5, 6, 3', 5'), 5.89 (bs, 1H, -OH), 4.50-4.41 (m, 1H, c'), 4.26-4.10 (m, 2H, c, d), 3.35-3.26 (m, 3H, a, e'), 3.02-2.92 (m, 5H, b, e, f), 1.97-1.78 (m, 2H, g), 1.06 (t, 3H, $J=7.40$, h); **^{13}C NMR data (δ , ppm)**: 201.00; 163.56, 156.88; 136.43; 134.34, 130.51; 129.62; 128.95; 127.91, 126.31; 121.08, 115.16; 114.74, 112.77, 71.12, 64.15, 50.75; 49.94, 43.46; 29.10, 18.92, 10.60; **LC-MS**: m/z = 360.10 ($M^+ + 1$), 116.13, 342.17, 98.13, 109.08, 283.08, 72.26; **HRMS**: Measured mass for $[M+H]^+$ is 360.19678, calculated mass for $C_{21}H_{26}FNO_3 + H^+$ is 360.19695

5f (**$C_{22}H_{30}ClNO_3$**): 3-(4-methyl-phenyl)-1-[2-(2-hydroxy-3-propylamino-propoxy)-phenyl]-propan-1-one hydrochloride salt. The white solid was recrystallized from mixture acetone/methanol 1:1. Yield: 73.7%; Melting point: 119.9-121.7 °C; **IR (ATR) (cm^{-1})**: 2968.1 (-NH-), 1661.7 (-C=O), 1594.1 (ArC-C-); **1H NMR data (δ , ppm)**: 8.27 (bs 1H, -NH), 7.70-7.65 (m, 1H, ArH 6'), 7.50-7.41 (m, 1H, ArH 4'), 7.10 (s, 4H, ArH: 2, 3, 5, 6), 7.05-6.97 (m, 2H, ArH: 3', 5'), 5.73 (bs, 1H, -OH), 4.62 (m, 1H, c'), 4.20-4.16 (m, 2H, c, d), 3.26-3.19 (m, 3H, a, e'),

2.99-2.87(m, 5H, e, b, f), 2.30 (s, 3H, Ar-CH₃), 1.96-1.74 (m, 2H, g), 1.00 (t, 3H, J=7,4, h); ¹³C NMR data (δ, ppm): 201.72; 157.06; 137.90; 135.54; 134.21; 130.58, 129.18; 128.20; 126.94; 121.17; 113.16; 71.21, 64.73, 51.11; 50.29, 44.05; 29.70, 20.83, 19.17, 11.05; **LC-MS**: m/z = 356.20 (M⁺+1), 116.13, 338.20, 105.11, 72.25, 98.15, 279.05; **HRMS**: Measured mass for [M+H]⁺ is 356.22145, calculated mass for C₂₂H₂₉NO₃+ H⁺ is 356.22202.

4.2. Bioassays

4.2.1. Preparation of samples solutions

Stock solutions of compounds were prepared in DMSO (Fluka, Chemie AG Buchs, Switzerland) at a concentration of 10 mM, filtered through Millipore filter (0.22 μm). Before use, and after wards diluted to various working concentrations with a nutrient medium (RPMI-1640, Sigma Chemical Co. St Louis, MO), supplemented with l-glutamine (3 mM), streptomycin (100 μg/ml) and penicillin (100 IU/ml), 10% heat inactivated (56 °C) fetal bovine serum (FBS, Sigma Chemical Co.) and 25 mM Hepes, (4-(2-hydroxyethyl)-1-piperazineethanesulfonic acid) adjusted to pH 7.2 by bicarbonate solution. MTT (3-(4,5-dimethylthiazol-2-yl)-2,5-diphenyl tetrazolium bromide) was dissolved (5 mg/ml) in phosphate buffer saline, pH 7.2, and filtered through Millipore filter, 0.22 μm, before use.

4.2.2. Cell culture

Human cervical carcinoma (HeLa cells), human melanoma (Fem-X), human prostate cancer (PC-3), human breast cancer (MCF-7), and human colon

carcinoma (LS174 cells) were cultured as a monolayer, while human chronic myelogenous leukemia (K562 cells) were grown in a suspension in the complete nutrient medium, at 37 °C in humidified air atmosphere with 5 % CO₂.

4.2.3. Treatment of tumor cell lines

HeLa (2,000 cells per well), Fem-X (2,000 cells per well), PC-3 (7,000 cells per well), MCF-7 cells (3,000 cells per well), LS174 (5,000 cells per well) were seeded into 96-well microtiter plates. Twenty hours later, after the cell adherence, five different concentrations of investigated compounds in complete nutrient medium were added to the wells, except for the control cells to which a nutrient medium only, was added. K562 cells were seeded at 3,000 per well, two hours before addition of investigated compounds to give desired final concentrations within the range mentioned above.

4.2.4. Preparation of peripheral blood mononuclear cells (PBMC)

PBMC were separated from whole heparinized blood (obtained from healthy volunteers) by Lymphoprep (Nycomed, Oslo, Norway) gradient centrifugation. Interface cells, washed three times with Haemacel (aqueous solution supplemented with 145 mM Na⁺, 5.1 mM K⁺, 6.2 mM Ca²⁺, 145 mM Cl⁻ and 35 g/L gelatin polymers, pH 7.4), were counted and resuspended in nutrient medium with 10 % FBS.

4.2.5. Treatment of PBMC from normal healthy donors

PBMC were seeded at the density of 150,000 cells per well in a nutrient medium only, or in a nutrient medium enriched with 5 µg/mL of phytohaemagglutinin (PHA-Welcome Diagnostics, England) in 96-well microtiter plates. Two hours later, five different concentrations of investigated compounds were added to the wells with non-stimulated and PHA stimulated PBMC.

4.2.6. Determination of cell survival

Cell survival was determined by MTT test according to the method of Mosmann [³¹], and modified by Ohno and Abe [³³], 72 h after the drug addition. Briefly, 20 µL of MTT solution, 5 mg/mL in phosphate buffered saline, was added to each well. Samples were incubated for further 4 h at 37 °C in humidified atmosphere with 5 % CO₂. Then, 100 µL of 10 % SDS was added to the wells. Absorbance was measured at 570 nm the next day. To get cell survival (S %), absorbance at 570 nm of a sample with cells grown in the presence of various concentrations of agent was divided with absorbance of control sample (the absorbance of cells grown only in nutrient medium), and multiplied by 100. It was implying that absorbance of blank was always subtracted from absorbance of a corresponding sample with target cells. Concentration IC₅₀ was defined as the concentration of a drug required for inhibiting cell survival by 50 %, compared with control. The results were generated from three independent experiments; each experiment was performed in triplicate. The selectivity (SI) was also calculated from the IC₅₀ ratio of normal epithelial and cancerous (HeLa, Fem-X, PC-3, MCF-7, LS174 and

K562) cells. SI value indicates selectivity of the sample to the cell lines tested. Samples with SI value greater than 3 were considered to high selectivity^[34].

4.3. Computational Methods

The QSAR study was started with the pKa calculation and selection of dominant microspecies at physiological pH for all examined compounds (Figure 2), using the Marvin Sketch 5.5.1.0 program^[34]. The Marvin 5.5.1.0 computational algorithms are based on the fundamental chemical structure theory to estimate a variety of chemical reactivity parameters.

Minimum energy conformations for dominant forms of all analyzed compounds (Scheme 1) were obtained by use of the Molecular Orbital PACKage/Parametric Method Vs.3 (MOPAC/PM₃) method^[36-37]. Molecular descriptors of optimized molecular models were computed by use of the Marvin Sketch 5.5.1.0^[35], Chem3D Ultra 7.0.0^[38], and Dragon 6 programs^[31]. The CS Gaussian 98 program^[39] using the B3LYP hybrid functional including 3-21G basis set (B3LYP/3-21G)^[40-42] was applied for computation of molecular parameters such as: Highest Occupied Molecular Orbital (HOMO) energy, Lowest Unoccupied Molecular Orbital (LUMO) energy, chemical potential, softness, hardness, electrophilicity and dipole. The calculated molecular descriptors were used for development of QSAR model by use of the Partial Least Square (PLS) Regression^[43]. The Soft Independent Modeling of Class Analogy SIMCA P+ 12.0 program^[44] was used for the PLS analysis and 2D-QSAR modelling.

Partial least square (PLS) regression, recently developed generalization of multiple linear regressions (MLR) ^[45], has been used for calculation of Variable Importance in the Projection (VIP) and QSAR models building. In multilinear modeling, a summary of the importance of each variable (x_k), for both Y and X matrices, is presented as VIP_k parameter. The x-variables with VIP value larger than 1 are the most relevant for explaining the regression model, the x-variables with $1.0 > VIP > 0.5$ are moderately influential, while x-variables with VIP value smaller than 0.5 are not relevant for the model ^[45]. Descriptors with lowest VIP-value are successively removed from the PLS model and new PLS model is created. For each new model are calculated regression factor R^2 , $Q^2(Y)$, F ratio, P-value, root mean square error of estimation (RMSEE), and compared with the previous model. The procedure is repeated until the best model is created.

Quality of the obtained 2D-QSAR models was examined by use of the leave-one-out cross-validation (R^2 , Q^2 and root mean square error of estimation (RMSEE)) ^[46], response permutation test (Y scrambling) ^[45], CV-ANOVA analysis of variance testing of cross-validated predictive residuals (F- and P-value) ^[47] and external validation (root mean square error of prediction (RMSEP) and $R^2_{Obs \text{ vs. } Pred}$).

Predictive power of the model is determined by Q^2 , which is leave-one-out cross-validated version of R^2 . A model is fitted to the data leaving one compound out, compute VIP, selects the best variables, and predicts Y for the left-out compound. This procedure is repeated until all compounds have been left out, which result in twelve parallel models. The difference between observed and the

predicted Y values are calculated ($e_{(i)}$) for each model. In this setting were defined PRESS (Predicted Sum of Squares), RMSEP and Q^2 as:

$$PRESS = \sum_{i=1}^n e_{(i)}^2 \quad (1)$$

$$RMSEP = \sqrt{\frac{PRESS}{n}} \quad (2)$$

$$Q^2(Y) = 1 - \frac{PRESS}{SSTo} \quad (3)$$

Variation, Sum of Squares (Total) - $SSTo$

PLS models with $Q^2 \geq 0.5$ can be considered to have good predictive capability^[48].

The response permutation test (Y scrambling) is applied in order to investigate the statistical significance of the R^2 and Q^2 and to test the model for overfitting due to the chance correlation^[43,45]. In this test the Y-matrix is randomly re-ordered (100 times in this project) while the X-matrix is kept intact. Model is fitted to the new Y-data and the new $R^2(Y)$, Q^2 and VIP parameters are calculated. All model selection steps are repeated on the scrambled Y-response data. Lines are fitted through the R^2 -values and through the Q^2 -values, yielding two separate intercepts. For a valid model, the R^2 - intercept should not exceed the 0.4 while the Q^2 -intercept < 0.05 ^[43, 45].

The F-test, based on the ratio MS Regression/MS Residual, formally assesses the significance of the model. The P-value indicates the probability level where a model with this F-value may be the result of just chance. The common practice is to interpret a P-value lower than 0.05 as pointing to a significant model^[47].

The 3D-QSAR studies of the chalcones were performed by use of the Pentacle 1.0.6 program ^[49], advanced software tool for obtaining alignment-independent 3D quantitative structure-activity relationships. The 3D-QSAR starts from computing highly relevant 3D maps of interaction energies (GRID based Molecular Interaction Fields-MIFs) between the examined molecule and four chemical probes: DRY (which represent hydrophobic interactions), O (sp² carbonyl oxygen, representing H-bond acceptor), N1 (neutral flat NH, like in amide, H-bond donor), and the TIP probe (molecular shape descriptor). The grid spacing was set to 0.5 Å and the MACC2 smoothing window to 1.6. The number of filtered nodes was set to 100 with 50% relative weights within the ALMOND discretization.

The interaction energy between the probe and the target molecule is calculated at each point as the sum of Lennard-Jones (E_{ij}), hydrogen bond (E_{hb}), electrostatic interactions (E_{el}), and an entropic term:

$$E_{xyz} = \sum E_{ij} + \sum E_{el} + \sum E_{hb} + S \quad [49].$$

Pentacle automatically encodes these maps into GRID Independent Descriptors (GRIND and GRIND2 descriptors) which are independent of the alignment of the series ^[50]. The GRIND approach aims to extract the information enclosed in the MIFs and compress it into new types of variables whose values are independent of the spatial position of the molecule studied by using an optimization algorithm with the intensity of the field at a node and the mutual node–node distances between the chosen nodes as a scoring function. Such variables constitute a matrix of descriptors that are analyzed using multivariate

techniques, such as Principal Component Analysis (PCA) and Partial Least Squares (PLS) regression analysis. The Principal Component Analysis was used for inspection of our series and for obtaining a map of our compounds describing their similarities and differences. The variables were used for development of 3D-QSAR models by use of the PLS regression ^[43].

The 3D-QSAR models were evaluated by use of the regression factor R^2 , the leave-one-out cross-validation parameter (Q^2) ^[46], RMSEE of the training set, RMSEP of the test set, and $R^2_{\text{Obs vs. Pred}}$ of the test set.

Acknowledgment

Financial support from the Serbian Ministry of Science (Grants 172041) is greatly appreciated. We also thank the Faculty of Chemistry and Faculty of Technology and Metallurgy, Belgrade University for their assistance.

References

1. Bach P.B. ; Jett J. R.; Pastorino U.; Tockman M. S.; Swensen S. J.; Begg C. B., Computed Tomography Screening and Lung Cancer Outcomes. *JAMA*, **2007**, 297, 953-962.
2. Zhuang H.;Weiwei J.;Wei C.; Kui Q.;Wei D.; Lin C.; Qilai H.;Shufeng Li; Fei D.; Jen-Fu C.; Xue-Xun F.; Min Lu; Zi-Chun H.; Down-regulation of HSP27 sensitizes TRAIL-resistant tumor cell to TRAIL-induced apoptosis. *Lung Cancer*, **2010**, 68, 27-38

3. Dyrager C.; Wickstroem M.; Friden-Saxin M.; Friberg A; Dahlen K.; Wallen E. A. A.; Gullbo J. Grotli M.; Luthman K. Inhibitors and promoters of tubulin polymerization: Synthesis and biological evaluation of chalcones and related dienones as potential anticancer agents. *Bioorganic & Medicinal Chemistry*, **2011**, 19, 2659-2665.
4. Batovska D. I.; Todorova T. I. Trends in Utilization of the Pharmacological Potential of Chalcones. *Current Clinical Pharmacology*, **2010**, 5, 1-29.
5. Pajeva I.K. ; Wiese M. A comparative Molecular Field Analysis of Propafenone-type Modulators of Cancer Multidrug Resistance. *Quant.Struct.-Act.Relat.*, **1998**, 17, 301-312.
6. Ecker G.; Chiba P.; Hitzler M.; Schmid D.; Visser K.; Cordes H.P.; Csöllei J.; Seydel J. K.; Schaper K.J. Structure-Activity Relationship Studies on Benzofuran Analogs of Propafenone-Type Modulators of Tumor Cell Multidrug resistance, *J.Med.Chem.*, **1996**, 39, 4767-4774.
7. Ruan B.F.; Lu X.; Tang J.F.; Wei Y.; Wang X.L.; Zhang Y.B.; Wang L.S.; Zhu HL. Synthesis, biological evaluation, and molecular docking studies of resveratrol derivatives possessing chalcone moiety as potential antitubulin agents., *Bioorg. Med. Chem.* **2011** 19, 2688-2695.
8. Manna F.; Chimenti F.; Bolasco A.; Bizzarri B.; Botta M.; Tafi A.; Filippelli A.; Rossi S. Synthesis and preliminary biological evaluation of 4,6-disubstituted 3-cyanopyridin-2(1H)-ones, a new class of calcium entry blockers. *Bioorg. Med. Chem. Lett.* **2000**, 10, 1883-1885.

9. Chimenti F.; Fioravanti R.; Bolasco A.; Chimenti P.; Secci D.; Rossi F.; Yáñez M.; Orallo F.; Ortuso F.; Alcaro S.; Cirilli R.; Ferretti R.; Sanna M.L. A new series of flavones, thioflavones, and flavanones as selective monoamine oxidase-B inhibitors. *Bioorg. Med. Chem.* **2010** 18, 1273-1279.
10. Albrecht F.; Mueller J.; Lietz H.; Wiersdorff W.W.; Hege H.G.; Mueller C.D.; Gries J.; Lenke D.; Von Philipsborn G.; Raschack M. Aminopropanol derivatives of 2-hydroxy-phenylpropiophenones, pharmaceutical compositions and use. U.S. ,**1985**, 10 pp. Cont. of U.S. Ser. No. 416,228, abandoned. CODEN: USXXAM US 4540697 A 19850910 CAN 104:109222 AN 1986:109222.
11. Dinkova-Kostova A.T.; Massiah M.A.; Bozak R.E.; Hicks R.J.; Talalay P. Potency of Michael reaction acceptors as inducers of enzymes that protect against carcinogenesis depends on their reactivity with sulfhydryl groups. *Proc.Natl.Aca.Sci. U.S.A.*, **2001**, 98, 3404-3409.
12. Anderson B. M.; Anderson C.D.; Donzelli G.; Dal Pozzo A. Sulfhydryl enzyme inactivation by nicotinoylacrylates. *Biochem.Biophys.Acta.*, **1984**, 703, 215-220.
13. Pati H.N.; Das U.; Ramirez-Erosa I.J.; Dunlop D.M.; Hickie R. A.; Dimmock J. R. α -Substituted 1-Aryl-3-dimethylaminopropanone Hydrochlorides: Potent Cytotoxins towards Human WiDr Colon Cancer Cells. *Chem. Pharm. Bull.* **2007**, 55 511—515.
14. Xia Y.; Yang Z.Y.; Xia P.; Bastow K. F.; Nakanishi Y.; Lee K.H. Antitumor Agents. Part 202: Novel 20-Amino Chalcones:Design, Synthesis and Biological Evaluation. *Bioorg. Med. Chem.Lett.* **2000**, 10, 699-701.

15. Li Q.; Sham H.L. Discovery and Development of Antimitotic Agents That Inhibit Tubulin Polymerization for the Treatment of Cancer. *Expert. Opin. Ther. Pat.* **2002**, 12, 1663-1702.
16. Bryson H.M.; Palmer K.J.; Langtry H.D.; Fitton A. Propafenone. A reappraisal of its pharmacology, pharmacokinetics and therapeutic use in cardiac arrhythmias. *Drugs*, **1993**, 45, 85-130.
17. Lowes D. J.; Guiguemde A.W.; Connelly M.C.; Zhu F.; Sigal M.S.; Clark J.A.; Lemoff A.S.; Derisi J.L.; Wilson E.B., Guy K.R. Optimization of Propafenone Analogues as Antimalarial Leads. *J. Med. Chem.* **2011**, 54, 7477–7485.
18. Chiba P.; Burghofer S.; Richter E.; Tell B.; Moser A.; Ecker G. Synthesis Pharmacologic Activity and Structure-Activity Relationships of a Series of Propafenone-Related Modulators of Multidrug Resistance. *J. Med. Chem.* **1995**, 38, 2789-2793.
19. Chiba P.; Tell B.; Jäger W.; Richter E.; Hitzler M.; Ecker G. Studies on propafenone-type Modulators of Multidrug-Resistance IV: Synthesis and Pharmacological Activity of 5-Hydroxy and 5-Benzoyloxy Derivatives. *Arch. Pharm. Pharm. Med. Chem.* **1997**, 330, 343-347.
20. Fiske J.L.; Fomin V.P.; Brown M.L.; Ducan R.L.; Sikes R.A. Voltage-sensitive ion channels in cancer. *Cancer Metastasis Rev.* **2006**, 25, 439-500.
21. Li M.; Xiong Z.G. Ion channels as targets for cancer therapy. *Int. J. Physiol. Pathophysiol. Pharmacol.* **2011**, 3, 156-166.
22. Le Guennec J.Y.; Ouadid-Ahidouch H.; Soriani O.; Besson P.; Ahidouch A.; Vandier C. Voltage-Gated Ion Channels, New Targets in Anti-Cancer Research. *Recent. Pat. Anticancer Drug Discov.* **2007**, 2, 189-202

23. Pardo L.A. Voltage-gated potassium channels in cell proliferation. *Physiology (Bethesda)*. **2004**, 19, 285-292.
24. Arcangeli A., Crociani O., Lastraioli E., Masi A., Pillozzi S. and Becchetti A, Targeting Ion Channels in Cancer: A Novel Frontier in Antineoplastic Therapy, *Curr Med Chem*. **2009**, 16, 66-93.
25. Arcangeli A.; Becchetti A. New Trends in Cancer Therapy: Targeting Ion Channels and Transporters. *Pharmaceuticals* **2010**, 3, 1202-1224.
26. Ecker G.; Chiba P.; Hitzler M.; Schmid D.; Visser K.; Cordes H.P.; Csöllei J.; Seydel J.K.; Schaper K.J. Structure-activity relationship studies on benzofuran analogs of propafenone-type modulators of tumor cell multidrug resistance. *J Med Chem*. **1996**, 39, 4767-74.
27. Pleban K.; Hoffer C.; Kopp S.; Peer M.; Chiba P. Intramolecular Distribution of Hydrophobicity Influences Pharmacologies; of Propafenone-type MDR Modulators. *Arch.Pharm.Pharm. Med. Chem*, **2004**, 337, 328-334.
28. Tmej C.; Chiba P.; Huber M.; Richter E.; Hitzler M.; Schaper K.-J.; Ecker G. A Combined Hansch/Free-Wilson Approach as Predictive Tool in QSAR Studies on Propafenone-Type Modulators of Multidrug Resistance. *Arch Pharm. (Weinheim)* **1998**, 331, 233-240.
29. Claisen L.; Claparede A. Condensation of ketones with aldehydes. *Ber. Deut. Chem. Ges.* 14, 2460-2480. From: *J. Chem. Soc., Abstr.* **1882**, 42, 511-513.
30. Ivković B, Vladimirov S, Novaković R, et al. The novel phenylpropiophenone derivatives induced relaxation of isolated rat aorta. *Arzneimittelforschung*. 2012,62(7):345-350.

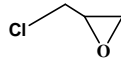
31. Dragon 6, TALETE srl, Via V. Pisani, 13 - 20124 Milano – Italy.
<http://www.taletе.mi.it>
32. Mosmann T. Rapid colorimetric assay for cellular growth and survival: application to proliferation and cytotoxicity assays. *J. Immunol. Methods*. **1983**, 65, 55-63.
33. Ohno M.; Abe T. Rapid colorimetric assay for the quantification of leukemia inhibitory factor (LIF) and interleukin-6 (IL-6). *J. Immunol. Methods*. **1991**, 145,199-203.
34. Mahavorasirikul W.; Viyanant V.; Chaijaroenkul W.; Itharat A.; Na-Bangchang K. Cytotoxic activity of Thai medicinal plants against human cholangiocarcinoma, laryngeal and hepatocarcinoma cells in vitro. *BMC Complement Altern. Med*. **2010**, 10:55
35. ChemAxon Marvin 5.5.1.0 program, Budapest, Hungary, **2011**.
www.chemaxon.com/products.html.
36. Stewart J. J. P.. Optimization of Parameters for Semi-Empirical Methods I-Method. *J. Comp. Chem.*, **1989**, 10:209-220.
37. Stewart J. J. P. "Optimization of parameters for semiempirical methods. II. Applications"; *J. Comput. Chem*. **1989**, 10, 221-264.
38. CS Chem3D Ultra 7.0, Cambridge Soft Corporation, (Property Picker ActiveX Control), 100 Cambridge Park Dr. Cambridge, MA 02140-2317 U.S.A., **2001**.
<http://www.cambridgesoft.com/>.
39. Gaussian 98 (Revision A.7), M. J. Frisch at al., Gaussian, Inc., Pittsburgh PA, **1998**.

40. Becke A.D., Density-functional thermochemistry. III. The role of exact exchange, *J. Chem. Phys.* , **1993**, 98, 5648-5652.
41. Lee C.; Yang W.; Parr R.G.; Development of the Colle-Salvetti correlation-energy formula into a functional of the electron density. *Phys. Rev. B Condens. Matter.* **1988**, 37, 785-789.
42. Roothaan C. C. J. New Developments in Molecular Orbital Theory. *Rev. Mod. Phys.*, **1951**, 23, 69-89.
43. Eriksson L.; Johansson E.; Kettaneh-Wold N.; Trygg J.; Wikstrom C.; Wold S. (Eds.) Multi-and Megavariate Data Analysis. Basic Principles and Applications I, 2nd ed., Umetrics Academy, Umeå, **2001**.
44. Umetrics AB, Umea, Sweden, SIMCA P+ program, Version 12.0.0.0, May 20. **2008**, www.umetrics.com
45. A. Tropsha, Best Practices for QSAR Model Development, Validation, and Exploitation. *Mol. Inf.* **2010**, 29, 476 – 488.
46. Allen, D.M. The relationship between variable selection and data auggmentation and a method for prediction. *Technometrics*, **1974**, 16, 125-127.
47. Ståhle, L.; Wold, S. Analysis of variance (ANOVA). *Chemometr. Intell. Lab. Syst.*, **1989**, 6, 259-272.
48. Wold, S.; Johansson, E.; Cocchi, M. 3D QSAR in drug design, theory, methods, and applications. H. Kubinyi Ed., ESCOM Science Publishers: Leiden, **1993**, pp 523–550.

49. Pentacle, Version 1.0.6; Molecular Discovery Ltd, Perugia, Italy, **2009**.
50. Pastor, M.; Cruciani G.; McLay I.; Pickett S.; Clementi S. *J. Med. Chem.* **2000**, 43, 3233-3243.

ACCEPTED MANUSCRIPT

List of Scheme

Scheme1. Synthetic route and structures of investigated 2'-hydroxy chalcones and propafenone derivatives: i-10% NaOH/C₂H₅OH/rt; ii-5%Pd/C,rt; iii-/NaOH; iv- *n*-CH₃CH₂CH₂NH₂; v-1M HCl

List of Figures

Figure 1. General structure and numbering of the chalcones and propafenone molecular scaffolds and its pharmacophoric group responsible for pharmacological activity.

Figure 2. The chemical structures of dominant forms at pH 7.4 of compounds used for external validation of 2D/3D-QSAR (HeLa), 2D/3D-QSAR (Fem-X) 2D/3D-QSAR (K562), 2D/3D-QSAR (MCF-7), 2D/3D-QSAR (PC-3) and 2D/3D-QSAR (LS174) models.

Figure 3. 3D-QSAR (HeLa) pharmacophore model for A) 5d and B) 5a. With red lines are presented descriptors with positive influence on the activity, while with blue lines are depicted variables with negative impact on the activity.

Figure 4. 3D-QSAR (Fem-X) pharmacophore model for A) 5b and B) 5e. With red lines are presented descriptors with positive influence on the activity, while with blue lines are depicted variables with negative impact on the activity.

Figure 5. 3D-QSAR (K562) pharmacophore model for A) 5a, B) 1a, and C) . With red lines are presented descriptors with positive influence on the activity, while with blue lines are depicted variables with negative impact on the activity.

Figure 6. 3D-QSAR (MCF-7) pharmacophore model A) . With red lines are presented descriptors with positive influence on the activity, while with blue lines are depicted variables with negative impact on the activity.

Figure 7. 3D-QSAR (PC-3) pharmacophore model A).. With red lines are presented descriptors with positive influence on the activity, while with blue lines are depicted variables with negative impact on the activity.

Figure 8. 3D-QSAR (LS174) pharmacophore model A). With red lines are presented descriptors with positive influence on the activity, while with blue lines are depicted variables with negative impact on the activity.

List of Tables

Table 1. Concentrations of investigated compounds which induced 50% decrease (IC_{50}) in malignant cell lines and peripheral blood mononuclear cell survival (without and with phytohemagglutinin). Results are obtained from two independent experiments performed in triplicate. Cisplatin was used as positive control

Table 2. The Selectivity index (SI) of investigated compounds as a ratio of IC_{50} values for peripheral blood mononuclear cells (PBMC), without or with phytohemagglutinin (PHA), and IC_{50} for malignant cell lines (HeLa, Fem-X, K562, MCF-7, PC-3 and LS174).

Table 3. Statistical parameters of QSAR models and prediction of pIC_{50} (HeLa) values for external validation set (HeLa-T1 to HeLa-T5). *Cytotoxic activities are shown as $pIC_{50} = (\log 1/IC_{50})$

Table 4. Statistical parameters of QSAR models and prediction of pIC_{50} (Fem-X) values for external validation set (FemX-T1 to FemX-T5). *Cytotoxic activities are shown as $pIC_{50} = (\log 1/IC_{50})$

Table 5. Statistical parameters of QSAR models and prediction of pIC_{50} (K562) values for external validation set (K562-T1 to K562 –T8). *Cytotoxic activities are shown as $pIC_{50} = (\log 1/IC_{50})$

Table 6. Statistical parameters of QSAR models and prediction of pIC_{50} (MCF-7) values for external validation set (MCF-7-T1 to MCF-7–T4). *Cytotoxic activities are shown as $pIC_{50} = (\log 1/IC_{50})$

Table 7. Statistical parameters of QSAR models and prediction of pIC_{50} (PC-3) values for external validation set (PC-3-T1 to PC-3-T4). *Cytotoxic activities are shown as $pIC_{50} = (\log 1/IC_{50})$

Table 8. Statistical parameters of QSAR models and prediction of pIC_{50} (LS174) values for external validation set (LS174-T1 to LS174-T13). *Cytotoxic activities are shown as $pIC_{50} = (\log 1/IC_{50})$

Compounds	IC ₅₀ ± S.D. (μM)							
	HeLa	Fem-X	K562	MCF-7	PC-3	LS174	PBMC	PBMC+PHA
1a	18.1±1.3	10.2±0.6	9.2±1.2	16.9±1.6	33.5±4.1	26.4±1.8	41.9±6.4	25.2±9.7
1c	8.9±1.7	8.7±1.4	4.8±0.6	14.4±2.2	21.6±3.5	17.4±0.6	17.6±4.5	16.4±3.1
1e	22.6±2.1	21.8±3.4	17.9±0.8	26.0±2.9	30.4±6.6	35.3±6.1	n.d.*	n.d.*
1b	14.7±2.7	22.4±3.7	18.5±4.4	37.7±4.3	19.2±2.4	48.8±2.4	n.d.*	n.d.*
1f	20.6±0.3	21.2±3.5	18.9±0.1	33.9±1.4	27.6±5.0	41.2±6.1	n.d.*	n.d.*
1d	11.2±1.8	10.4±2.8	9.8±1.4	29.8±6.9	20.1±2.8	32.2±1.2	n.d.*	n.d.*
5a	6.78±1.61	16.1±1.1	8.8±0.2	9.7±1.6	23.3±0.9	18.6±0.3	44.4±1.3	35.5±1.2
5c	16.42±0.46	38.2±3.0	37.6±2.9	18.5±1.2	46.4±1.2	72.2±0.2	47.5±1.0	48.1±4.1
5e	16.1±3.2	9.6±1.1	27.7±7.5	33.0±1.3	31.9±6.6	23.2±0.9	60.3±5.4	48.8±3.6
5b	8.9±2.1	6.8±0.8	8.1±2.9	23.4±1.1	18.0±1.2	20.3±0.2	52.4±3.5	49.8±5.1
5f	21.7±3.1	12.7±3.0	14.7±4.7	31.7±3.4	24.7±2.8	20.8±0.6	48.7±6.7	41.4±3.2
5d	3.0±1.5	4.9±0.0	6.0±1.5	20.2±4.3	12.6±2.4	11.2±0.3	59.5±3.2	52.9±3.2
Cisplatin	2.6±0.0	5.7±0.3	4.7±0.3	n.d.	n.d.	n.d.	33.3±0.0	26.6±0.0

n.d.* -Not determined

Table 1. Concentrations of investigated compounds which induced 50% decrease (IC₅₀) in malignant cell lines and peripheral blood mononuclear cell survival (without and with phytohemagglutinin). Results are obtained from two independent experiments performed in triplicate. Cisplatin was used as positive control.

Compounds	Selectivity Index											
	PBMC/ HeLa	PBMC+PHA/ HeLa	PBMC/ Fem-X	PBMC+PHA/ Fem-X	PBMC/ K562	PBMC+PHA/ K562	PBMC/ MCF-7	PBMC+PHA/ MCF-7	PBMC/ PC-3	PBMC+PHA/ PC-3	PBMC/ LS174	PBMC+PHA/ LS174
1a	2.31	1.92	4.10	3.42	4.55	3.79	2.48	2.07	1.25	1.04	1.59	1.32
1c	1.98	1.84	2.02	1.88	3.67	3.41	1.22	1.14	0.81	0.76	1.01	0.94
5a	6.55	5.24	2.76	2.20	5.05	4.03	4.58	3.66	1.91	1.52	2.39	1.91
5c	2.89	2.93	1.24	1.26	1.26	1.28	2.57	2.60	1.02	1.04	0.66	0.67
5e	3.75	3.03	6.28	5.08	2.18	1.76	1.83	1.48	3.35	1.53	2.60	2.10
5b	5.89	5.60	7.71	7.32	6.47	6.15	2.24	2.13	2.91	2.77	2.58	2.45
5f	2.24	1.91	3.83	3.26	3.31	2.82	1.54	1.31	1.97	1.68	2.34	1.99
5d	19.83	17.63	12.14	10.80	9.91	8.82	2.95	2.62	4.72	4.20	5.31	4.72

Table 2. The Selectivity index (SI) of investigated compounds as a ratio of IC₅₀ values for peripheral blood mononuclear cells (PBMC), without or with phytohemagglutinin (PHA), and IC₅₀ for malignant cell lines (HeLa, Fem-X, K562, MCF-7, PC-3 and LS174).

Statistical parameters		2D-QSAR model	3D-QSAR model
R^2		0.824	0.97
$Q^2(Y)$		0.772	0.75
RMSEE (Training set)		0.103	0.054
External validation			
		2D-QSAR-Predicted	3D-QSAR-Predicted
Test Set	pIC ₅₀ (HeLa)*	pIC ₅₀ (HeLa)	pIC ₅₀ (HeLa)
HeLa-T1	5.027	5.04065	5.148
HeLa-T2	4.782	4.98954	4.892
HeLa-T3	5.229	5.08728	5.247
HeLa-T4	4.767	5.02235	5.184
HeLa-T5	4.828	5.24894	5.093
RMSEP (Test set)		0.179	0.232
$R^2_{\text{Obs vs. Pred}}$ (Test set)		0.003	0.383

Table 3. Statistical parameters of QSAR models and prediction of pIC₅₀ (HeLa) values for external validation set (HeLa-T1 to HeLa-T5). *Cytotoxic activities are shown as pIC₅₀= (log1/IC₅₀)

Statistical parameters		2D-QSAR model	3D-QSAR model
R^2		0.647	0.98
$Q^2(Y)$		0.585	0.58
RMSEE (Training set)		0.144	0.056
External validation			
		2D-QSAR-	3D-QSAR-
Test Set	pIC ₅₀ (Fem-X)*	Predicted pIC ₅₀ (Fem-X)	Predicted pIC ₅₀ (Fem-X)
FemX-T1	4.663	5.200	4.867
FemX-T2	4.622	5.247	4.885
FemX-T3	4.613	5.528	4.915
FemX-T4	5.009	5.521	4.914
FemX-T5	5.284	4.894	4.911
RMSEP (Test set)		0.621	0.265
$R^2_{\text{Obs vs. Pred}}$ (Test set)		0.281	0.254

Table 4. Statistical parameters of QSAR models and prediction of pIC₅₀ (Fem-X) values for external validation set (FemX-T1 to FemX-T5). *Cytotoxic activities are shown as pIC₅₀= (log1/IC₅₀)

Statistical parameters		2D-QSAR model	3D-QSAR model
	R^2	0.639	0.93
	$Q^2(Y)$	0.587	0.62
	RMSEE (Training set)	0.155	0.052
External validation			
		2D-QSAR-Predicted	3D-QSAR-Predicted
Test Set	pIC ₅₀ (K562)*	pIC ₅₀ (K562)	pIC ₅₀ (K562)
K562-T1	5.137	4.744	4.801
K562-T2	5.310	4.849	4.770
K562-T3	4.903	4.889	5.020
K562-T4	4.590	4.766	5.061
K562-T5	4.759	4.850	4.742
K562-T6	4.818	4.756	4.938
K562-T7	5.031	4.907	4.944
K562-T8	4.951	4.825	4.872
	RMSEP (Test set)	0.235	0.288
	$R^2_{\text{Obs vs. Pred}}$ (Test set)	0.054	0.299

Table 5. Statistical parameters of QSAR models and prediction of pIC₅₀ (K562) values for external validation set (K562 - T1 to K562 -T8). *Cytotoxic activities are shown as pIC₅₀= (log1/IC₅₀).

Statistical parameters		2D-QSAR model	3D-QSAR model
R^2		0.822	0.95
$Q^2(Y)$		0.812	0.80
RMSEE (Training set)		0.071	0.030
External validation			
Test Set		2D-QSAR-	3D-QSAR-
	pIC ₅₀ (MCF-7)*	Predicted pIC ₅₀ (MCF-7)	Predicted pIC ₅₀ (MCF-7)
MCF7-T1	4.764	4.792	4.541
MCF7-T2	4.975	4.983	4.572
MCF7-T3	4.625	4.781	4.487
MCF7-T4	5.000	4.808	4.596
RMSEP (Test set)		0.124	0.314
$R^2_{\text{Obs vs. Pred}}$ (Test set)		0.357	0.947

Table 6. Statistical parameters of QSAR models and prediction of pIC₅₀ (MCF-7) values for external validation set (MCF-7-T1 to MCF-7-T4). *Cytotoxic activities are shown as pIC₅₀ = (log1/IC₅₀)

Statistical parameters		2D-QSAR model	3D-QSAR model
R^2		0.851	0.96
$Q^2(Y)$		0.591	0.75
RMSEE (Training set)		0.055	0.018
External validation			
		2D-QSAR-	3D-QSAR-
Test Set	pIC ₅₀ (PC-3)*	Predicted pIC ₅₀ (PC-3)	Predicted pIC ₅₀ (PC-3)
PC3-T1	4.735	4.459	4.857
PC3-T2	4.475	4.653	4.441
PC3-T3	4.345	4.595	4.601
PC3-T4	4.910	4.794	4.576
RMSEP (Test set)		0.214	0.219
$R^2_{\text{Obs vs. Pred}}$ (Test set)		0.104	0.119

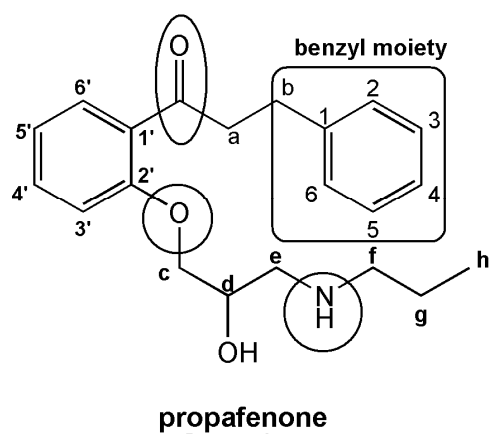
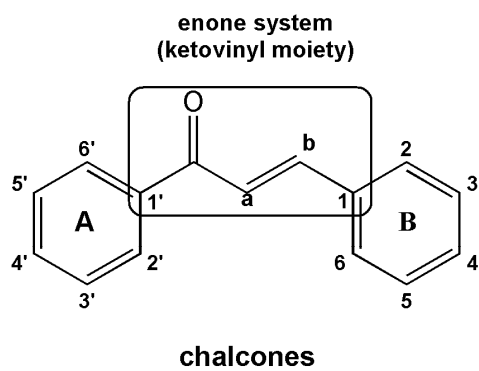
Table 7. Statistical parameters of QSAR models and prediction of pIC₅₀ (PC-3) values for external validation set (PC-3-T1 to PC-3-T4). *Cytotoxic activities are shown as pIC₅₀=(log1/IC₅₀).

Statistical parameters		2D-QSAR model	3D-QSAR model
R ²		0.609	0.96
Q ² (Y)		0.555	0.76
RMSEE (Training set)		0.133	0.057
External validation			
Test Set	pIC ₅₀ (LS174)*	2D-QSAR-Predicted pIC ₅₀ (LS174)	3D-QSAR-Predicted pIC ₅₀ (LS174)
LS174-T1	4.342	4.231	4.443
LS174-T2	4.546	4.295	4.457
LS174-T3	4.677	4.414	4.612
LS174-T4	4.591	4.247	4.690
LS174-T5	4.917	4.435	4.436
LS174-T6	4.755	4.330	4.581
LS174-T7	4.908	4.698	4.652
LS174-T8	4.558	4.359	4.436
LS174-T9	4.471	4.351	4.432
LS174-T10	4.543	4.409	4.424
LS174-T11	4.567	4.359	4.420
LS174-T12	4.490	4.227	4.437
LS174-T13	4.463	4.333	4.443
RMSEP (Test set)		0.266	0.177
R ² _{Obs vs. Pred} (Test set)		0.534	0.231

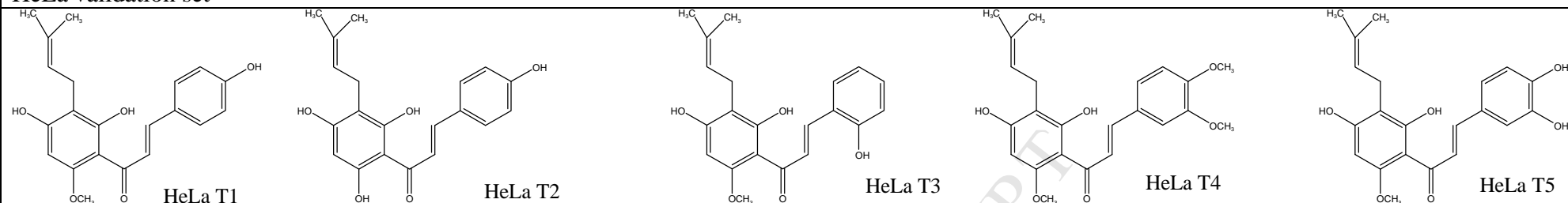
Table 8. Statistical parameters of QSAR models and prediction of pIC₅₀ (LS174) values for external validation set (LS174-T1 to LS174-T13). *Cytotoxic activities are shown as pIC₅₀= (log1/IC₅₀).

Highlights: Phenylpropiophenone derivatives as anticancer agents

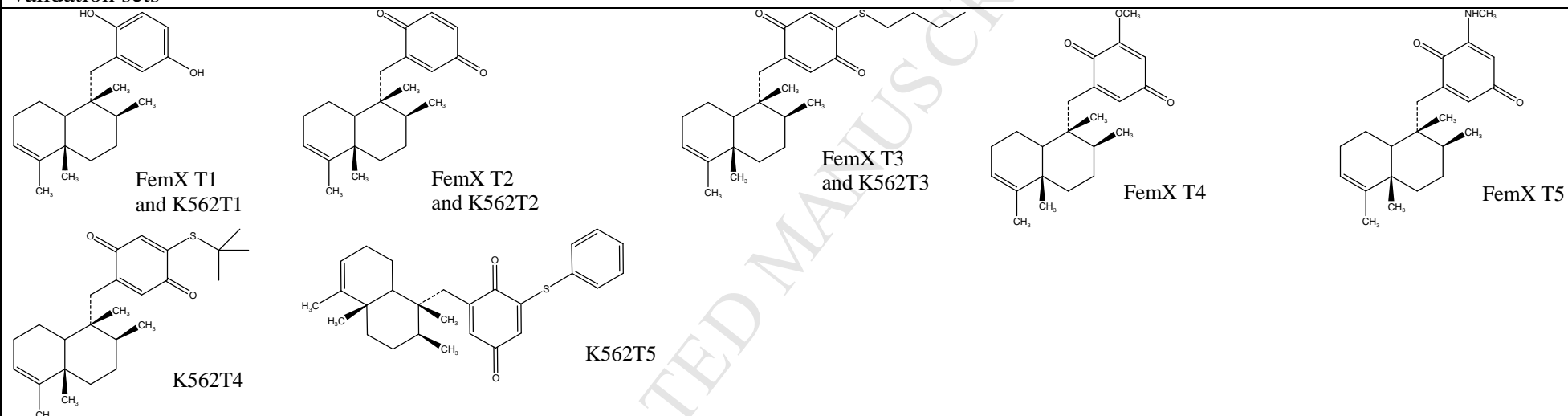
- Synthesis of novel phenylpropiophenone derivatives
- evaluation of their anticancer activities against six different cancer cell lines
- 2D and 3D-QSAR studies were performed for all compounds with cytotoxic activities
- QSAR studies have selected the significant molecular descriptors and pharmacophores



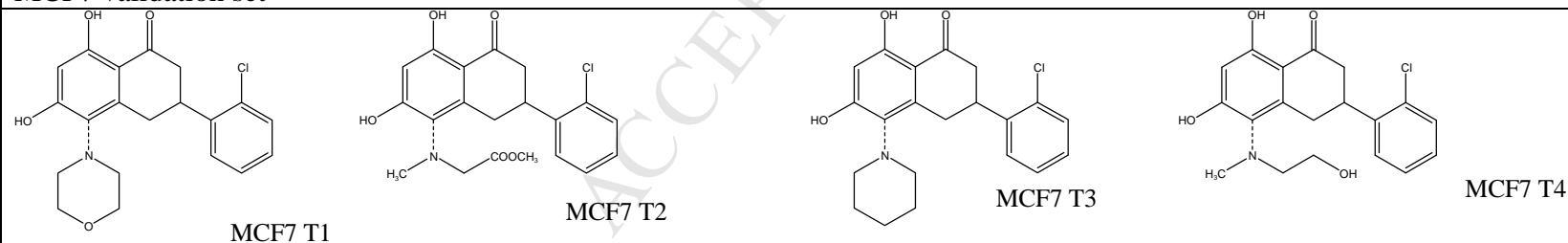
HeLa validation set



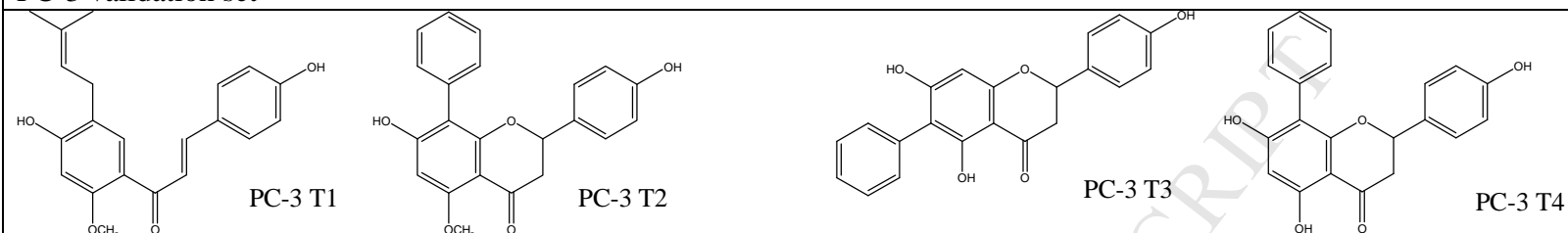
FemX and K562 validation sets



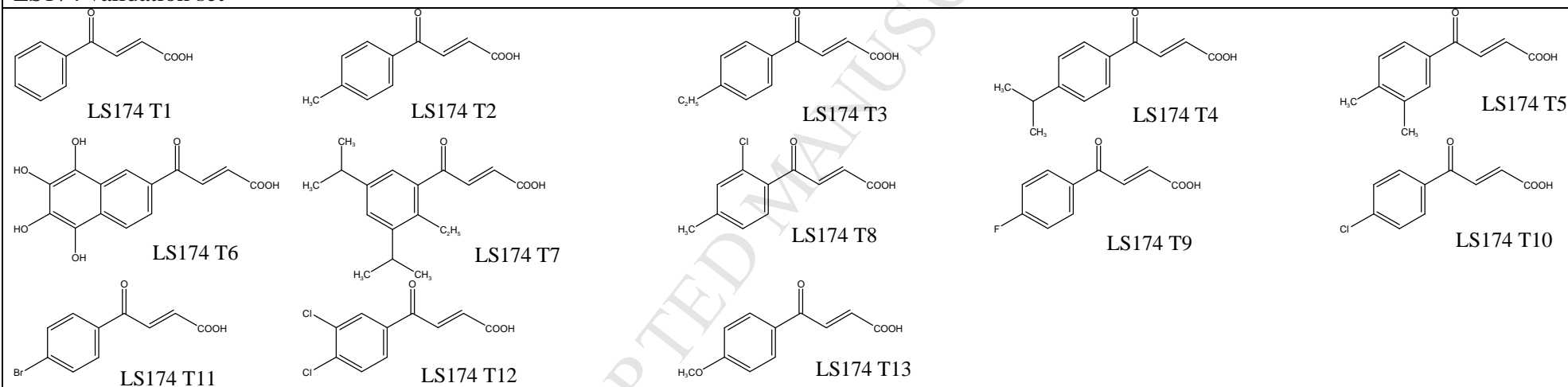
MCF7 validation set

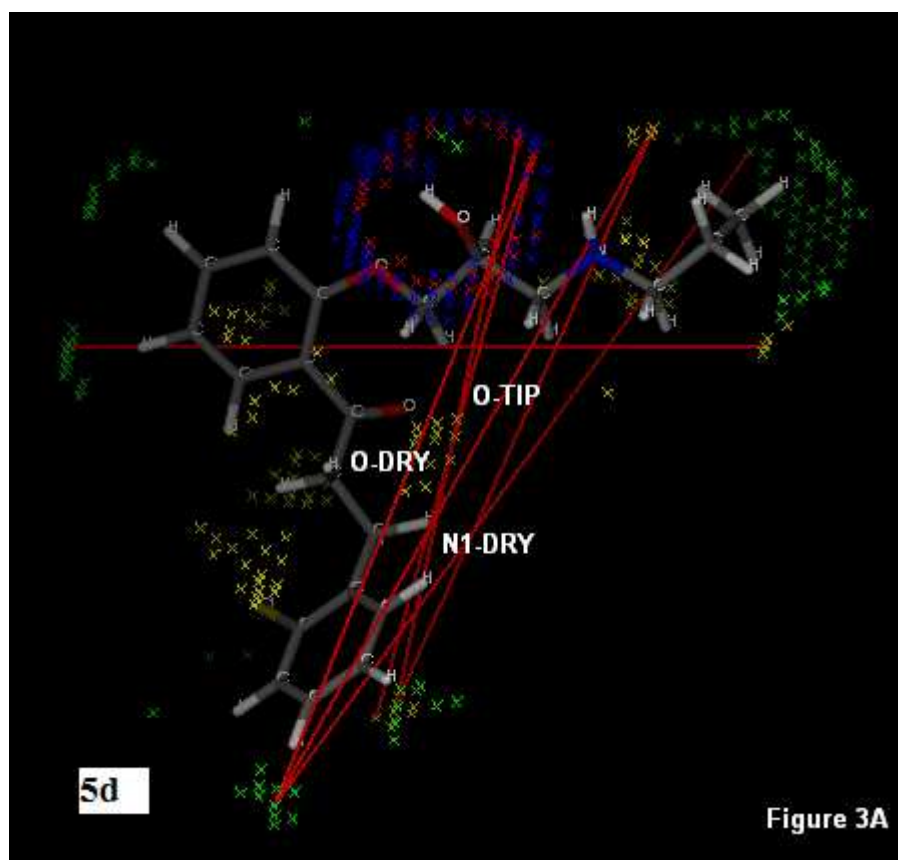


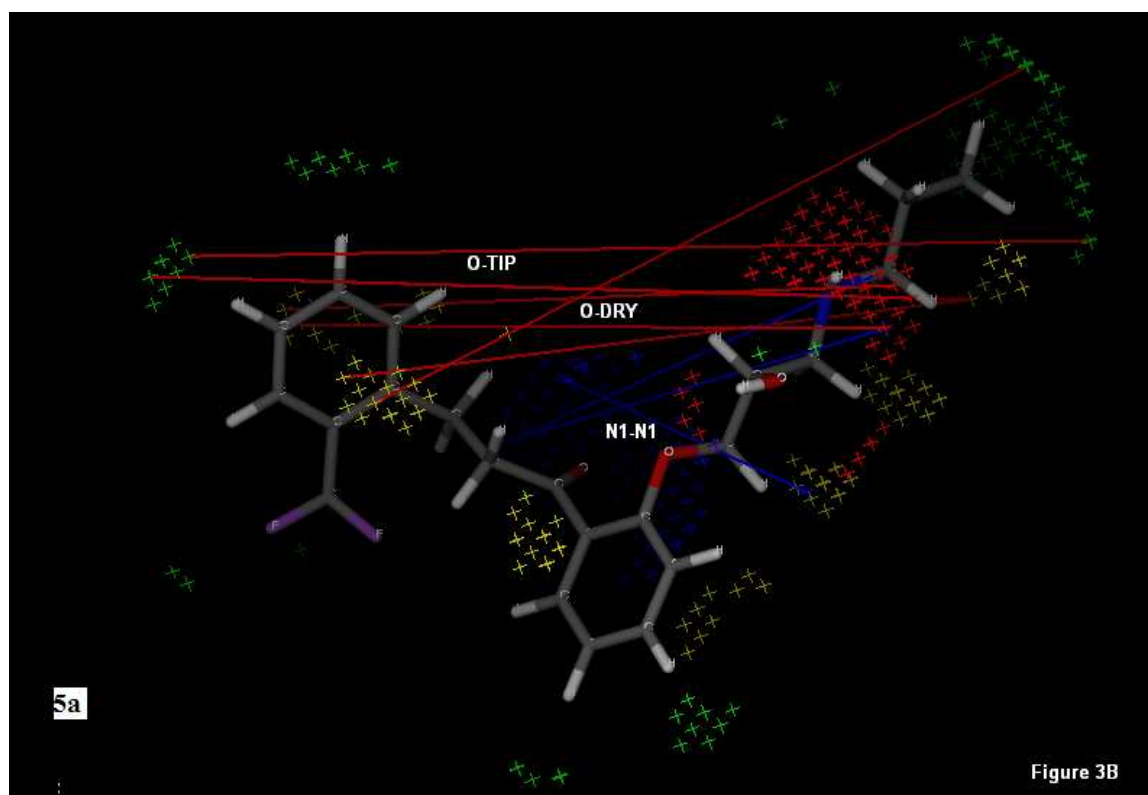
PC-3 validation set

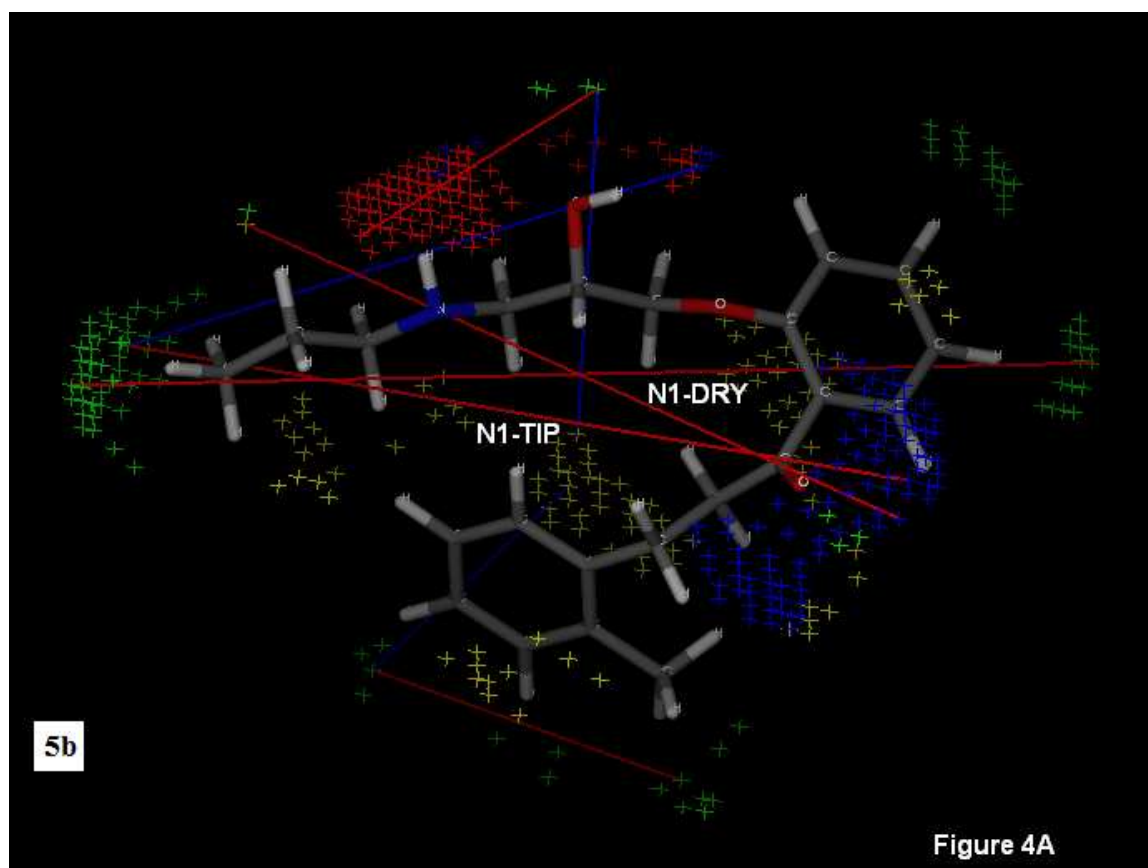


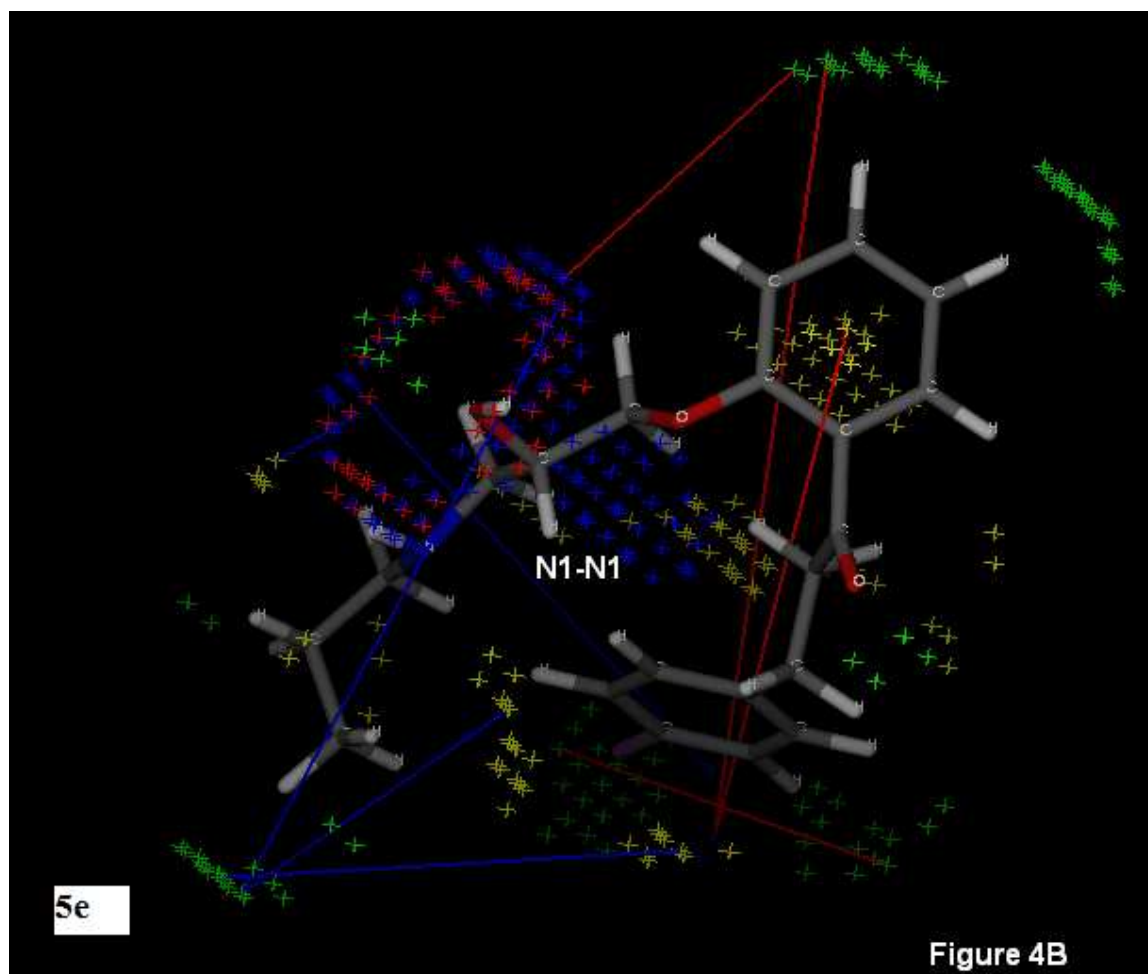
LS174 validation set

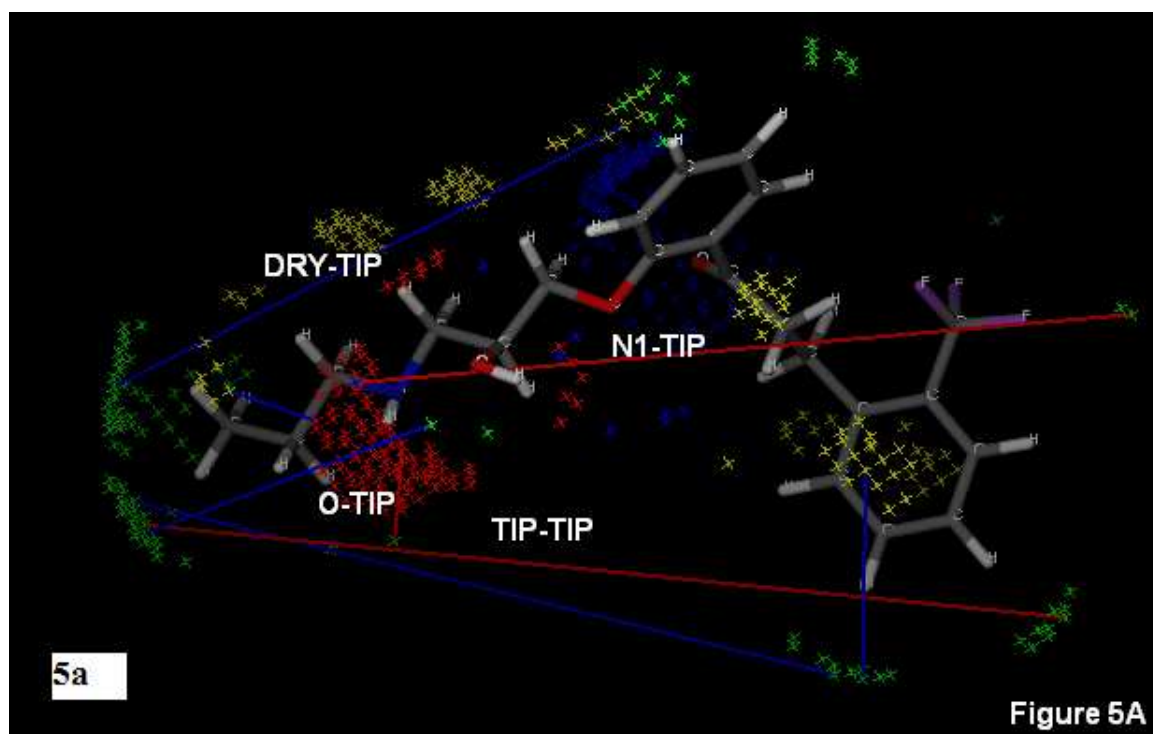


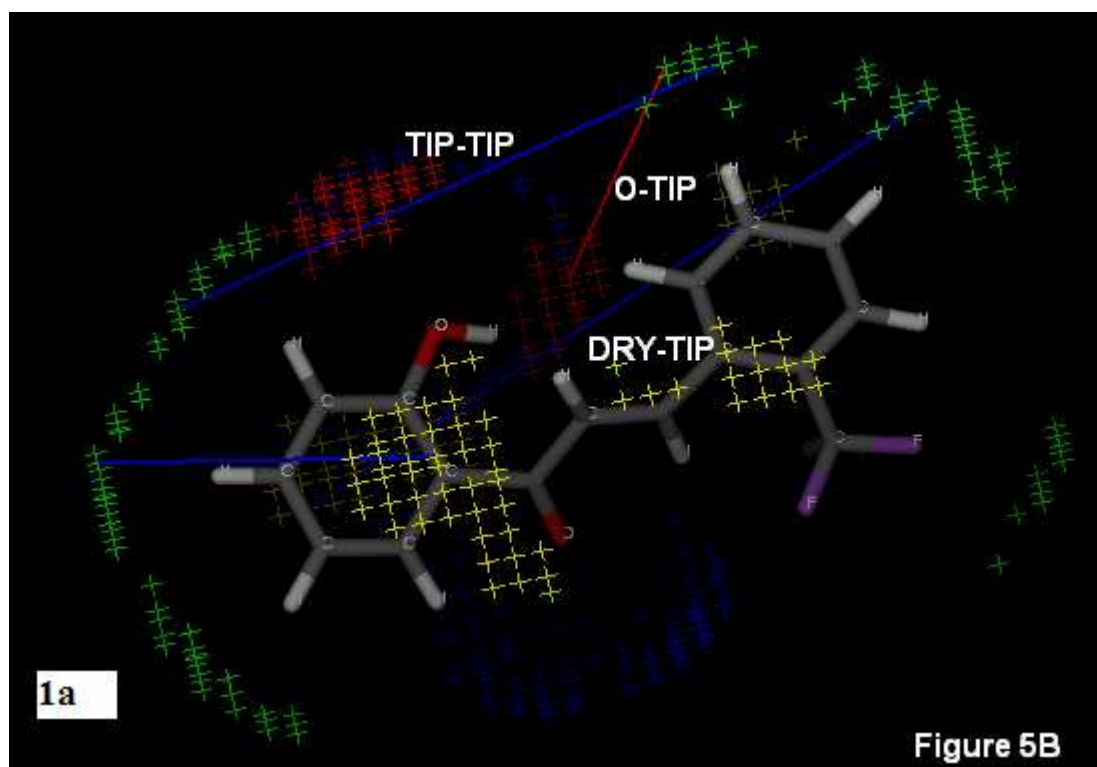


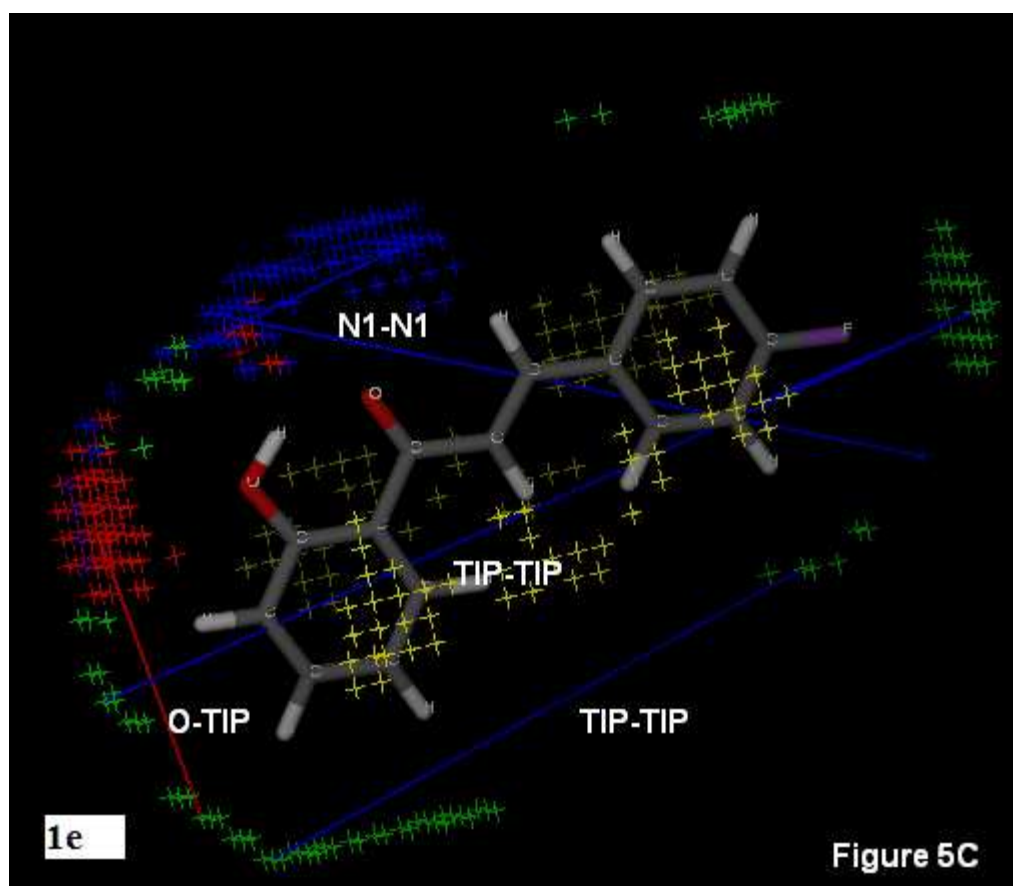


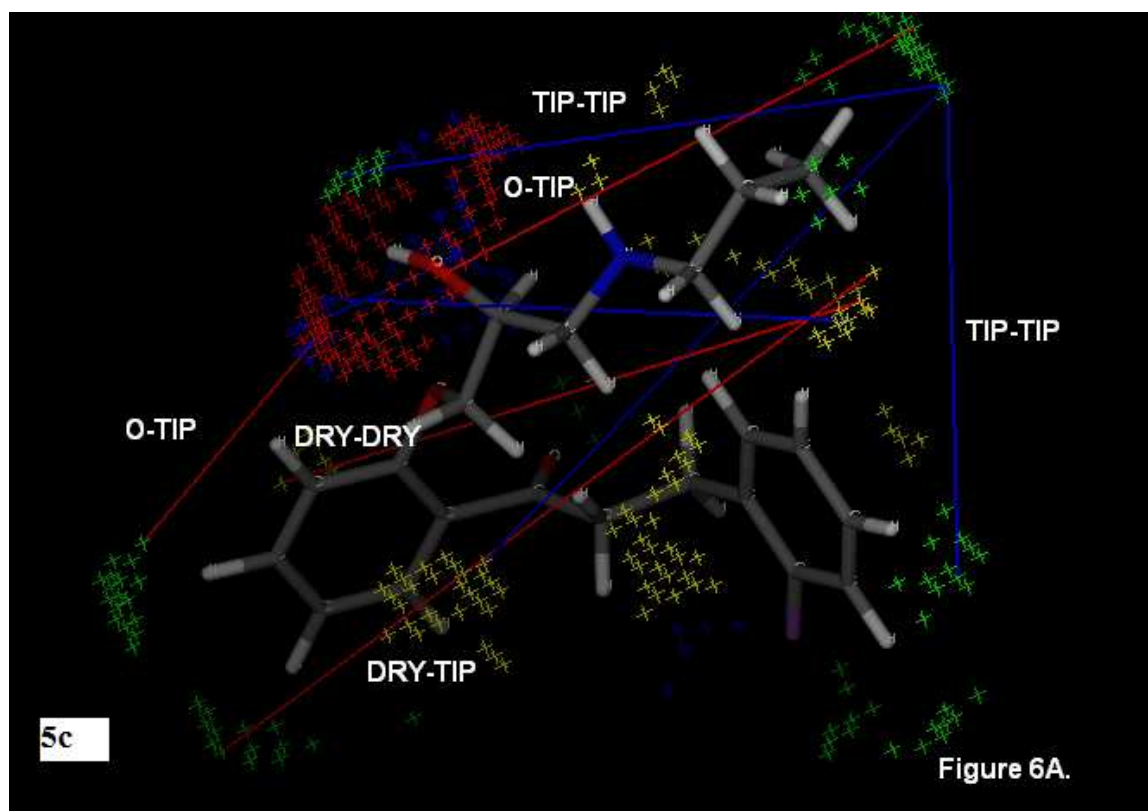


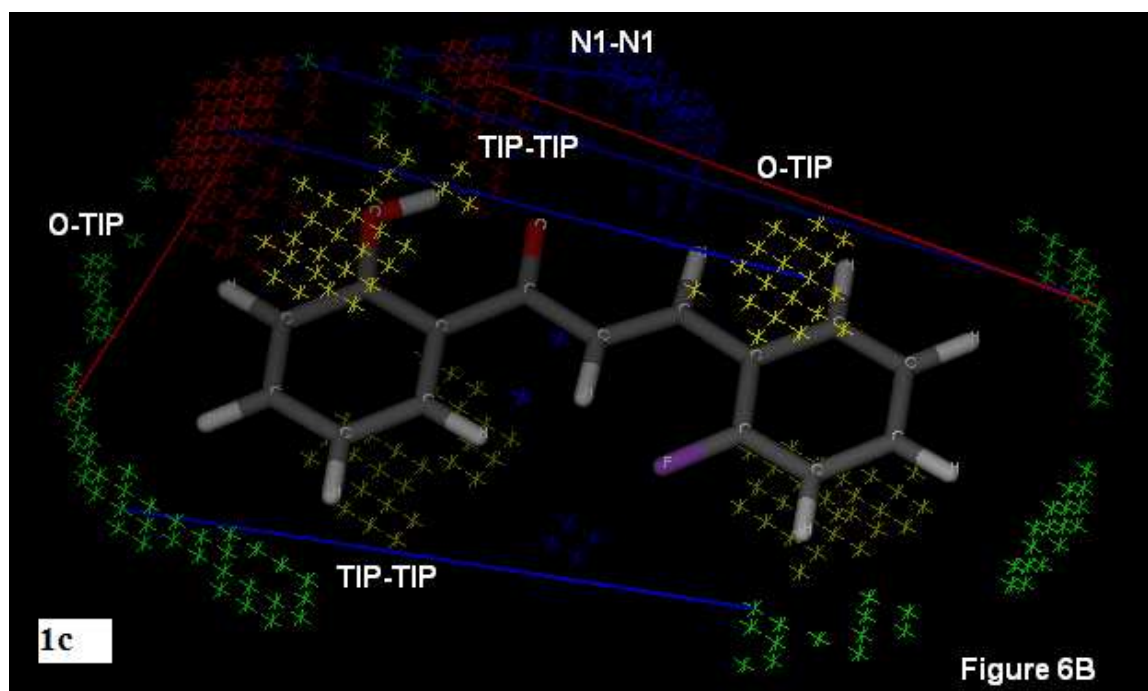


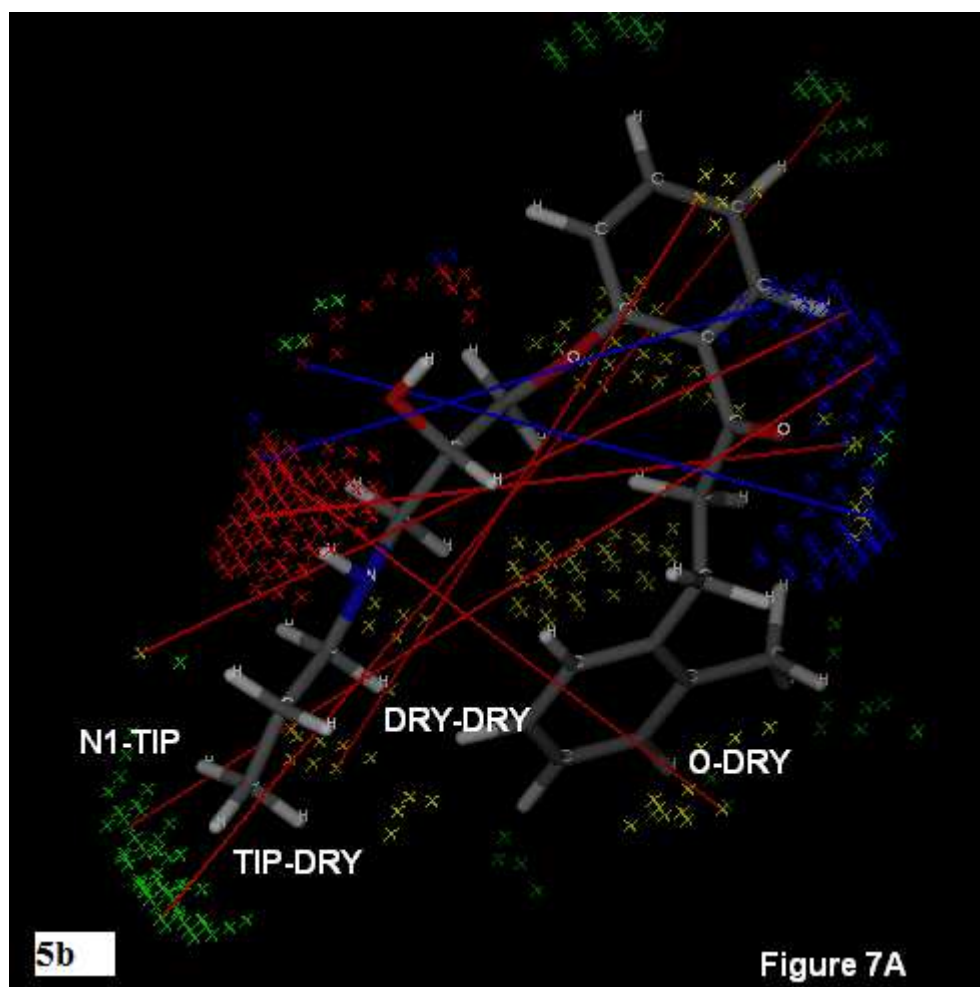


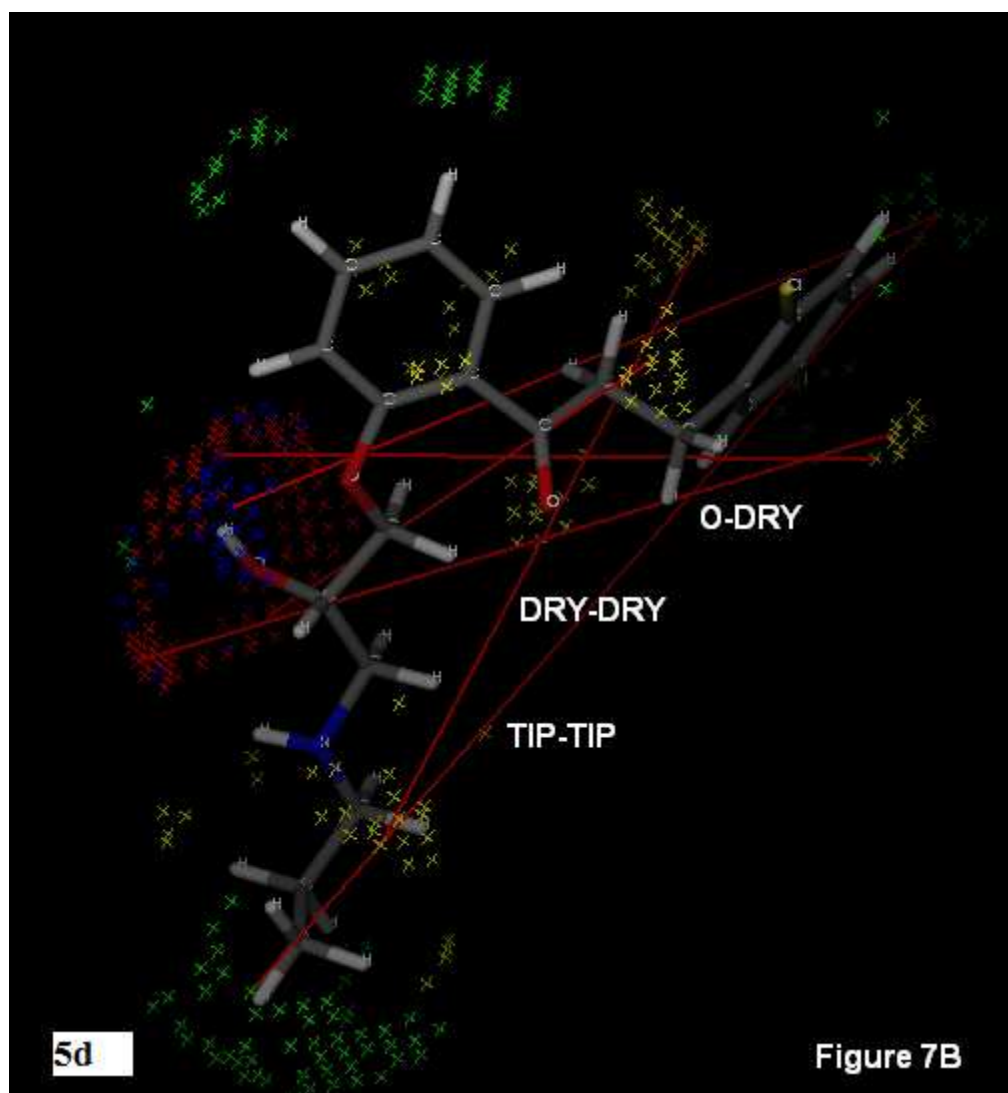


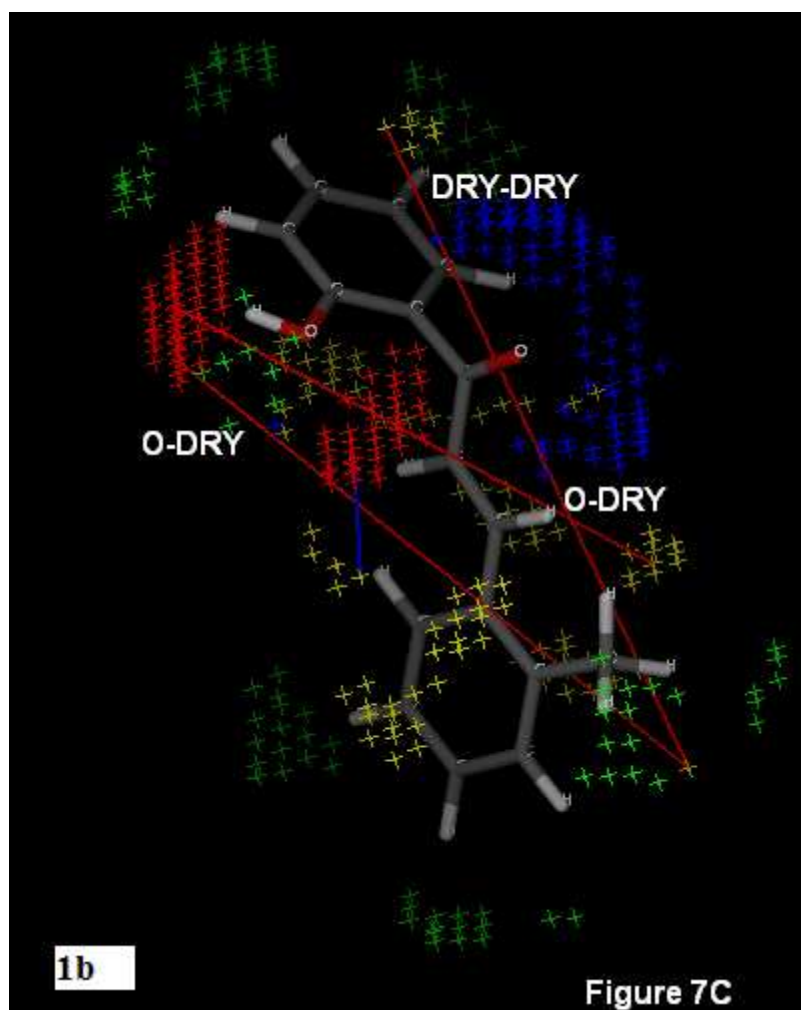


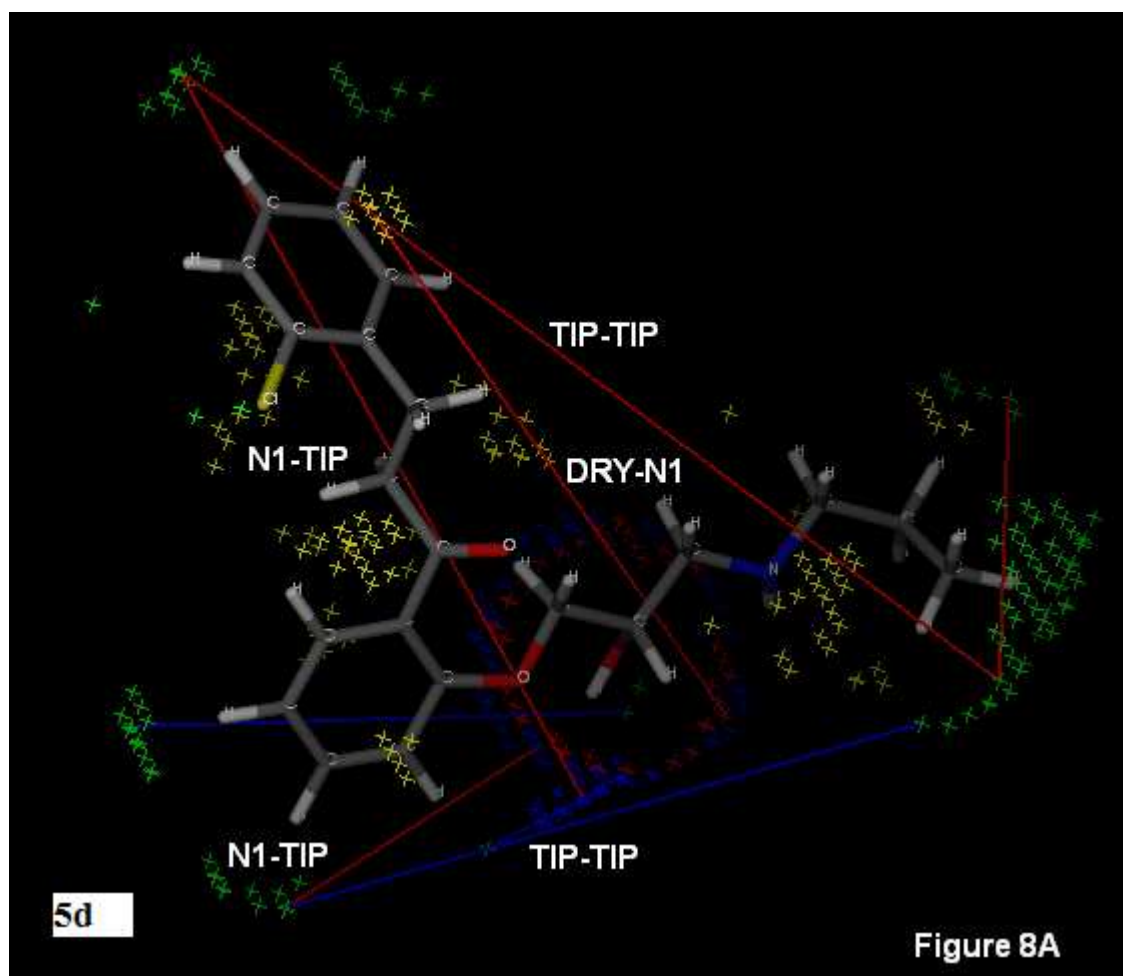


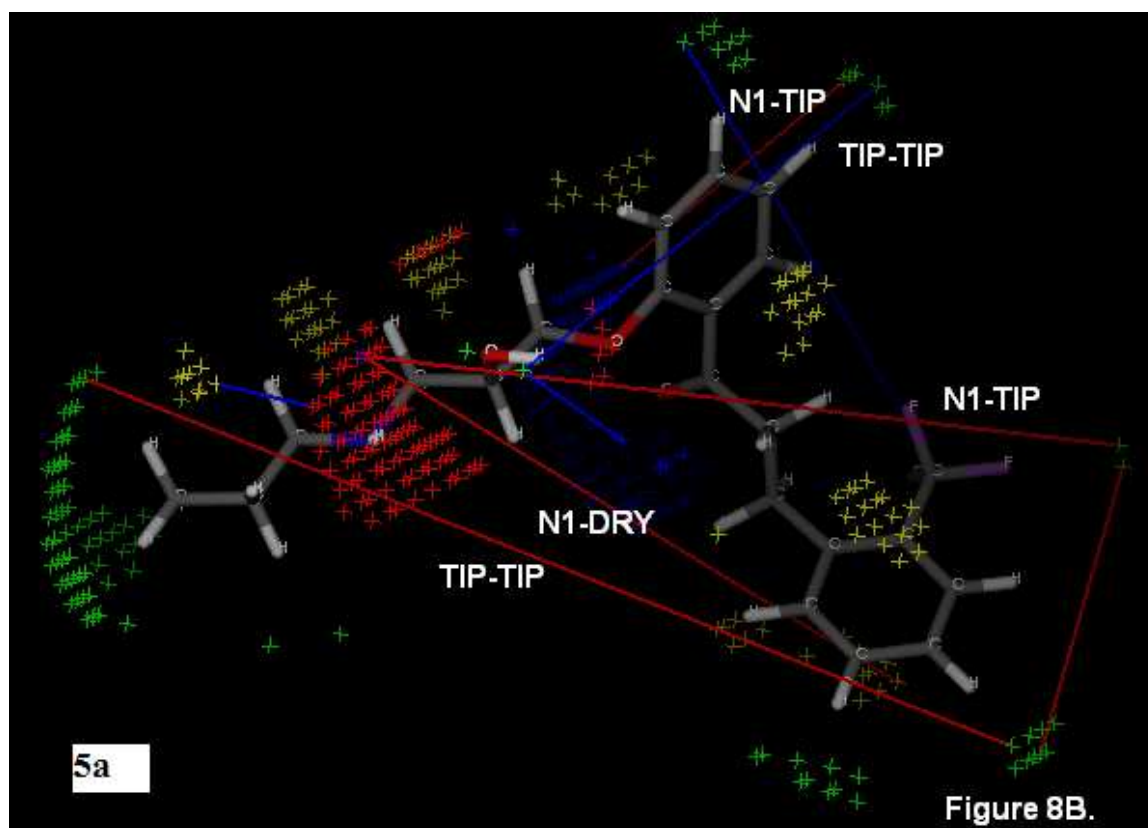


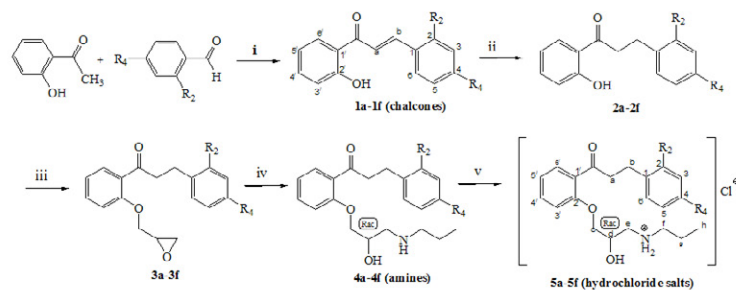












	1a-5a	1b-5b	1c-5c	1d-5d	1e-5e	1f-5f
R₁	-CF ₃	-CH ₃	-F	-Cl	-H	-H
R₂	-H	-H	-H	-H	-F	-CH ₃